

# High-precision sulfur isotope composition of enstatite meteorites and implications of the formation and evolution of their parent bodies

C. Defouilloy, Pierre Cartigny, N. Assayag, Frédéric Moynier, Jean-Alix Barrat

► **To cite this version:**

C. Defouilloy, Pierre Cartigny, N. Assayag, Frédéric Moynier, Jean-Alix Barrat. High-precision sulfur isotope composition of enstatite meteorites and implications of the formation and evolution of their parent bodies. *Geochimica et Cosmochimica Acta*, Elsevier, 2015, 172, pp.393-409. 10.1016/j.gca.2015.10.009 . insu-01455080

**HAL Id: insu-01455080**

**<https://hal-insu.archives-ouvertes.fr/insu-01455080>**

Submitted on 6 Aug 2020

**HAL** is a multi-disciplinary open access archive for the deposit and dissemination of scientific research documents, whether they are published or not. The documents may come from teaching and research institutions in France or abroad, or from public or private research centers.

L'archive ouverte pluridisciplinaire **HAL**, est destinée au dépôt et à la diffusion de documents scientifiques de niveau recherche, publiés ou non, émanant des établissements d'enseignement et de recherche français ou étrangers, des laboratoires publics ou privés.

1 **High-precision sulfur isotope composition of enstatite meteorites and implications of the**  
2 **formation and evolution of their parent bodies**

3

4 C. Defouilloy<sup>a,b, 1,2</sup>, P. Cartigny<sup>a</sup>, N. Assayag<sup>a</sup>, F. Moynier<sup>c, d</sup>, J.-A. Barrat<sup>e</sup>

5 <sup>a</sup>Géochimie des Isotopes Stables, Institut de Physique du Globe de Paris, Sorbonne Paris Cité,  
6 Univ. Paris Diderot, UMR 7154 CNRS, 1 rue Jussieu, 75238 Paris, France

7 <sup>b</sup>Laboratoire de Minéralogie et Cosmochimie du Muséum, Muséum National d'Histoire  
8 Naturelle, Paris, UMR 7202, 61 rue Buffon, 75005, Paris, France

9 <sup>c</sup>Cosmochimie, Astrophysique et Géophysique Expérimentale, Institut de Physique du Globe  
10 de Paris, Sorbonne Paris Cité, Univ. Paris Diderot, UMR 7154 CNRS, 1 rue Jussieu, 75238 Paris,  
11 France

12 <sup>d</sup>Institut Universitaire de France, Paris, France

13 <sup>e</sup>U.B.O.-I.U.E.M., CNRS UMR 66538 (Domaines Océaniques), Place Nicolas Copernic, 29280  
14 Plouzané Cedex, France

15

16 <sup>1</sup>Current address: WiscSIMS, Department of Geoscience, University of Wisconsin-Madison,  
17 Madison, WI 53706, USA

18 <sup>2</sup>Corresponding author. defouilloy@ipgp.fr

19

20

21 **Abstract**

22

23 In order to better understand the formation and evolution of their parent bodies, the three  
24 isotope ratios of sulfur were analyzed in 33 enstatite meteorites (24 enstatite chondrites and

25 9 aubrites). The results show that on average all enstatite chondrite groups are enriched in  
26 the lightest isotopes compared to other chondrite groups, with means of  $\delta^{34}\text{S}$  of  $-0.28 \pm$   
27  $0.22 \text{ ‰}$  for EH3/4,  $-0.16 \pm 0.16 \text{ ‰}$  for EH5,  $-0.32 \pm 0.15 \text{ ‰}$  for EL3,  $-0.67 \pm 0.16 \text{ ‰}$  for EL6  
28 and  $-0.64 \pm 0.00 \text{ ‰}$  for EL7 (all  $1\sigma$ ). Aubrites show a larger isotope variability in their  
29 composition, with a  $\delta^{34}\text{S}$  varying from  $-1.350\text{‰}$  to  $+0.154 \text{ ‰}$ . Contrary to previously  
30 published results, our data show a distinct composition for EL6 compared to other enstatite  
31 chondrites. This could be related to an impact-induced loss of isotopically heavy oldhamite  
32 ( $\delta^{34}\text{S} =$  by  $3.62 \pm 3.02 \text{ ‰}$  ( $1\sigma$ )) on the EL parent body. Although the bulk sulfur in both  
33 enstatite meteorites and aubrites does not show any significant  $\Delta^{33}\text{S}$  and  $\Delta^{36}\text{S}$ , the oldhamite  
34 fraction shows clear evidence of mass independent fractionation on the  $^{36}\text{S}/^{32}\text{S}$  ratio (in 3  
35 out of 9 analyzes,  $\Delta^{36}\text{S}$  up to  $+2.2\text{‰}$ ), a signal that is not correlated to any  $^{33}\text{S}/^{32}\text{S}$  anomaly (in  
36 1 out of 9 analyzes,  $\Delta^{33}\text{S}$  down to  $-0.085\text{‰}$ ). Though a nebular or photochemical origin  
37 cannot be ruled out, the most plausible mechanism to produce such isolated non-mass  
38 dependent  $^{36}\text{S}/^{32}\text{S}$  anomalies would be a contribution of  $\text{FeCl}_2$  containing excesses of  $^{36}\text{S}$  due  
39 to the decay of  $^{36}\text{Cl}$  to the leached oldhamite fraction. Even though the sulfur isotopic  
40 composition measured in enstatite meteorites is distinct from the Bulk Silicate Earth (BSE),  
41 the isotopically lightest samples of EL6, EL7 and aubrites are approaching the isotopic  
42 composition of the BSE and enstatite meteorites remain the meteorites with the sulfur  
43 isotopic composition the closest to the terrestrial one.

44

45

46

47 **1. INTRODUCTION**

48

49 Enstatite meteorites comprise two groups of meteorites: enstatite chondrites, which are  
50 undifferentiated (primitive) meteorites, and aubrites, which are also referred to as enstatite  
51 achondrites, and are differentiated material.

52

53 As shown by their mineral assemblages and compositions enstatite meteorites are the most  
54 reduced meteorites (Mason 1965, Keil 1968, Rubin 1984, Brett & Keil 1986, Weisberg &  
55 Kimura 2012, Barrat et al. 2014). This is attested by their major silicate phase which is near-  
56 pure enstatite ( $\approx 50$  wt% of total sample), with FeO < 1%. Their amount of FeNi metal ( $\approx 25$   
57 wt%) is higher than in other chondrite groups and the metal phase contains up to 2 wt% Si.  
58 Other important phases include troilite and plagioclase. The exceptionally reduced  
59 environment of their formation leads most lithophile elements to behave as chalcophile (El  
60 Goresy, 1988), and therefore to the formation of a large variety (0.1 to 1 %) of unusual  
61 sulphides, including oldhamite (CaS), niningerite ([Mg, Fe, Mn]S), alabandite (MnS) and rare  
62 minerals such as osbornite (TiN), sinoite ( $\text{Si}_2\text{N}_2\text{O}$ ), daubreelite ( $\text{FeCr}_2\text{S}_4$ ), caswellsilverite  
63 ( $\text{NaCrS}_2$ ) and perryite ( $[\text{Ni,Fe}]_8[\text{Si,P}]_3$ ) are further illustration of their very reduced character.

64

65

66 The enstatite chondrites are commonly subdivided into 2 sub-groups according to their  
67 amount of metallic Fe: EH (Fe-rich enstatite chondrites) and EL (Fe-poor enstatite  
68 chondrites) (Keil 1968, Sears 1980, Kallemeyn & Wasson 1983). It is also worth noting that  
69 EH are characterised by the occurrence of alabandite, while EL contain niningerite instead as  
70 well as various alkali sulfides (Lin & El Goresy 2002, Weisberg & Kimura 2012). In addition,  
71 Lin & El Goresy (2002) have given several petrographic evidence that the EH parent body had  
72 to form in even more reduced conditions than the EL parent body, with a lower oxygen and

73 a higher  $H_2S$  fugacity, resulting in a higher Si content in kamacite and perryite, and alkali  
74 enrichment in sulphides in unequilibrated EL3 compared to their EH3 counterparts. Like  
75 other chondrites, enstatite chondrites present various degrees of metamorphism, from the  
76 more primitive group, noted 3, to the most metamorphosed, noted 6 (or 7). Yet, due to their  
77 very specific mineralogies, it can be challenging to assess precisely the exact degree of  
78 metamorphism and uncertainty remains regarding the classification of enstatite chondrites  
79 (Quirico et al. 2011). It is to be noted that there are no hydrous metamorphosed enstatite.  
80 This is primarily the consequence that no hydrous phase exists, H being dissolved in the  
81 metal phase.

82

83 Interestingly, enstatite chondrites are the only undifferentiated meteorites to possess a well-  
84 identified differentiated counterpart, the aubrites. Aubrites are for the most part fragmental  
85 breccias or regolith impact breccias, with the exception of 6 samples representing impact  
86 melts (Casanova et al. 1993, Lorenzetti et al. 2002, Miura et al. 2007). Besides enstatite, their  
87 main minerals are albitic plagioclase, diopside and forsterite. Based on similar O isotopic  
88 compositions and major element content, they are thought to originate from an enstatite  
89 chondrite-like parent body, but neither from the EH nor the EL parent bodies (Keil 2010). No  
90 study has reported a comparison of O fugacity in aubrites with EL and EH. However, their  
91 mineralogical composition and possibly complementary Zn isotopic composition tends to  
92 show that aubrites are closer to EL than EH (Watters & Prinz 1979, Rubin 1984, Moynier et al.  
93 2011).

94

95 The origin of enstatite meteorites and their parent bodies and the genetic relationships  
96 between all the sub-groups remain partially unsolved today. There are several arguments in

97 favour of a common origin of enstatite chondrites. For example, they have several  
98 remarkable features that distinguish them from any other meteorite groups. They have a  
99 distinct mineralogy, with a wide variety of sulfides and metals, reflecting their highly reduced  
100 environments of formation. They also have similar oxygen isotopic compositions (Clayton &  
101 Mayeda 1996, Herwartz et al. 2014). It is therefore likely that they share a common origin.  
102 Several authors have favoured a common parent body for all the enstatite chondrites, EL  
103 and EH (Clayton and Mayeda, 1996, Kong et al. 1997). This is corroborated by the fact that  
104 they are all completely dry (there are no enstatite chondrites of petrologic types 1 or 2) and  
105 the high melting temperature of enstatite. Yet some incompatibilities have been emphasized  
106 (Keil 1968, Brett & Keil 1986, Lin & El Goresy 2002, Keil 2010). In particular, Lin and El Goresy  
107 (2002) showed that the chemical and petrography of the EH and EL were incompatible with  
108 a common parent body. EH have a higher Mg/Si ratio than the EL (Keil et al. 1968). EL and EH  
109 also have very distinct cooling rates and heating histories, suggesting distinct parent bodies  
110 (Zhang et al. 1995, Lin & El Goresy 2002).

111

112 The chemical, and isotopic similarities between enstatite meteorites that were previously  
113 used as evidence for common parent body are now re-interpreted in terms a common  
114 environment of formation for the different parent bodies (as attested by the mineralogy of  
115 the meteorites. Rubin et al. 2009). Even though it is now generally assumed that enstatite  
116 meteorites originate from at least four different parents bodies – one for the EL, one for the  
117 EH, and 2 for the aubrites (one for the Shallowater meteorite, and another parent body for  
118 all the other aubrites) – a few studies have pointed out the peculiarity of EL6 compared to  
119 EL3 and EH in their REE content (Rubin et al. 2009, Barrat et al. 2014) and zinc isotopic

120 composition (Moynier et al. 2011), leading to the question whether they could originate  
121 from an additional distinct parent body.

122

123 Both enstatite meteorites and the Earth (as well as other terrestrial planets) formed in a  
124 reduced environment, which suggests a possible link between them (Javoy et al. 2010,  
125 Sanloup et al. 1999). Isotopic similarities between the Earth and enstatite meteorites are  
126 remarkable, the most striking observation being the oxygen isotopic composition (Clayton et  
127 al. 1984, Clayton & Mayeda 1996, Newton et al. 2000, Herwartz et al. 2014). Isotopic  
128 similarity between the Earth and enstatite meteorites now extend to many additional  
129 elements such as Zn (Moynier et al. 2011), N (Javoy & Pineau 1983, Cartigny et al. 1997), Mo  
130 (Dauphas et al. 2004), Ru (Dauphas et al. 2004), Cr (Birck et al. 1999, Trinquier et al. 2007a),  
131 Sr (Moynier et al. 2010, 2012), Ti (Trinquier et al. 2007b) and Ca (Valdes et al. 2014). These  
132 similarities has led to the idea that, contrary to first assumptions, the Earth was not built  
133 from a majority of ordinary chondrites and carbonaceous chondrites -like material, but  
134 primarily from enstatite-like material (Javoy 1998, Javoy et al. 2010). However, the Mg/Si  
135 ratio of bulk enstatite chondrites is much lower than that of BSE, and the Si isotopic ratio  
136 measured in all enstatite meteorites is significantly different from Earth (Fitoussi & Bourdon  
137 2012, Savage & Moynier 2013), though Dauphas et al. (2015) have recently shown that  
138 Mg/Si ratio was dictated by the the condensation sequence of forsterite in the solar nebula.  
139 Earth and enstatite meteorites might also slightly differ in their Ti isotopic composition  
140 (Trinquier et al. 2009, Zhang et al. 2012) as well as Ca isotopic composition (Simon &  
141 DePaolo 2010), though the latter was recently proved disputable by Valdes et al. (2014).  
142 Finally, a recent study by Herwartz et al. (2014) revealed small but significant differences in  
143 the  $^{17}\text{O}$  isotopic compositions of Earth and enstatite meteorites:  $59 \pm 8$  ppm ( $0.059 \pm$

144 0.008 ‰) for EL and  $35 \pm 10$  ppm ( $0.035 \pm 0.01$  ‰) for EH. Though it seems undeniable that  
145 enstatite meteorites share a lot of features with the Earth, building the Earth solely from  
146 enstatite-like material is not free of difficulties.

147

148 Sulfur is present in enstatite meteorites in significant quantity ( $\approx 4$ -5 wt% S) (Keil et al. 1968).  
149 Having 4 isotopes ( $^{32}\text{S}$ ,  $^{33}\text{S}$ ,  $^{34}\text{S}$ ,  $^{36}\text{S}$ ), it allows the distinction of equilibrium and kinetic effects  
150 and the identification of mass independent isotopic fractionation (MIF). A scarce number of  
151 sulfur isotopic compositions have been measured in enstatite chondrites (Gao & Thiemens  
152 1993a) and aubrites (Rai et al. 2005), including significant MIF reported in the aubrite Norton  
153 County (Rai et al. 2005). To better discuss the differences and relationships between the  
154 different groups of enstatite meteorites and to better apprehend the link between the  
155 enstatite meteorites and the building material of the Earth, we report the S isotopic  
156 composition of 33 enstatite chondrites and aubrites, to create a precise spectrum of the S  
157 isotopic variations and possible MIF in all the enstatite-bearing bodies.

158

159

## 160 **2. SAMPLES AND METHODS**

161

162 33 samples of enstatite meteorites, from all groups and metamorphism degrees have been  
163 analysed: 2 EL3 (Mac 88 136, Mac 02 837), 9 EL6 (Hvittis, Khaipur, Eagle, North West Forest,  
164 Lon 94 100, Happy Canyon, EET 92 063, NWA 974, Pillistfer, Atlanta, Blithfield), 2 EL7 (Happy  
165 Canyon, Ilafegh 009), 8 EH3 (Indarch, Qinz-Zhan, Gro 95 517, Abee, Kota-Kota, Alha 77 295,  
166 Mil 07 028, Itqiy, Sahara 97 096), 3 EH5 (St Sauveur, LA 02 225, St Mark's) and 9 Aubrites  
167 (Norton County, Khor Temiki, Shallowater, Bishopville, Cumberland Falls, Aubres, Bustee,



168 Mayo Belwa, Pena Blanca). Two samples, North West Forest (EL6) and Itqiy (EL7-an), did not  
169 release any sulfur.

170

171

## 172 **2.1. Analytical techniques**

173

### 174 2.1.1. Extraction of reduced sulfur

175

176 Samples were obtained either as fine powders or as cm-size chunks of rocks that were  
177 subsequently crushed into powder. For bulk reduced sulfur extraction about 20 mg of  
178 powder was used in each experiment. When enough material was available, a replica or two  
179 were processed. The powdered samples were poured in a glass reaction vessel with 20 ml of  
180 chrome reduction solution ( $\approx 30\% \text{ Cr(III)Cl}_3 + 15\% \text{ Zn} + 55\% \text{ HCl } 0.6 \text{ N}$ , see Canfield et al.  
181 1986). 5 ml of HCl 6N were added to the mixture to ensure an acidic condition, which  
182 enhances the reaction rate. The flasks were heated to boiling temperature for 3 hours under  
183 a flux of  $\text{N}_2$ . Hydrogen sulfide was swept out with a stream of nitrogen gas, washed in  
184 distilled water, and collected in a silver nitrate solution.  $\text{Ag}_2\text{S}$  was rinsed with distilled water  
185 and then dried for 24 hours.

186

187 As detailed previously (e.g. Canfield et al. 1986) extensive tests on pure  $\text{FeS}_2$  original  
188 material has shown that our settings for the chemical extraction of sulfides ensure a close to  
189 100% yield and do not create any significant fractionation of sulfur isotopes.

190

191 Weighed aliquots of Ag<sub>2</sub>S samples wrapped in Al foils, are introduced in nickel bombs,  
192 evacuated and fluorinated with purified F<sub>2</sub> at 250° overnight. The reaction releases SF<sub>6</sub> which  
193 is then purified by cryogenic separation and gas chromatography (1/8 in. diameter column of  
194 a 6 ft 5A molecular sieve followed by a 8 ft Haysep Q column. Ono et al 2006). Purified SF<sub>6</sub> is  
195 then quantified using a capacitance manometer (to check for fluorination yield) and  
196 analyzed by mass spectrometry.

197

198 Several large samples were obtained, allowing the isotopic composition of oldhamite (CaS)  
199 to be investigated. CaS is a fragile sulphide, easily reacting with water to produce H<sub>2</sub>S. The  
200 extraction procedure was similar to the protocol used for extracting all sulphides: 3 g of  
201 powdered sample were poured in a flask, heated at ≈ 100°C for 10 hours with 20 ml of pure  
202 water. No other reagent was added. Particular care was taken to ensure that all glassware  
203 was perfectly dry before experiment. Similarly to bulk S extraction, H<sub>2</sub>S was produced and  
204 converted to Ag<sub>2</sub>S.

205

## 206 **2.2. Isotope analysis**

207

208 The sulfur isotopic compositions were measured using a dual inlet Thermo Finnigan MAT 253  
209 Mass Spectrometer at the Institut de Physique du Globe de Paris, France. M/z ratios 127,  
210 128, 129 and 131 ratios were monitored simultaneously (respectively for <sup>32</sup>SF<sub>5</sub><sup>+</sup>, <sup>33</sup>SF<sub>5</sub><sup>+</sup>, <sup>34</sup>SF<sub>5</sub><sup>+</sup>,  
211 <sup>36</sup>SF<sub>5</sub><sup>+</sup>). The δ<sup>34</sup>S values are calculated after calibration of our in-house SF<sub>6</sub> tank, using the  
212 international standard IAEA-S1 recommended value of Robinson (1993). As this reference  
213 material is anchored to V-CDT, the δ<sup>34</sup>S values measured in this study are all given respect to

214 V-CDT. There is no international calibration for neither  $\Delta^{33}\text{S}$  nor  $\Delta^{36}\text{S}$  and there are given with  
215 respect to our  $\text{SF}_6$  tank and were recalculated accordingly via the relations:

216  
217

$$218 \quad \Delta^{33}\text{S} = \delta^{33}\text{S} + 1000 \times [(\delta^{34}\text{S}/1000 + 1)^{0.515} - 1] \quad (1)$$

219

$$220 \quad \Delta^{36}\text{S} = \delta^{36}\text{S} + 1000 \times [(\delta^{34}\text{S}/1000 + 1)^{1.9} - 1] \quad (2)$$

221  
222

223 The quality of the measurements is estimated on the basis of the long term reproducibility of  
224 IAEA-S1 and IAEA-S2 reference materials (Table 1, Appendix A). Repeated analyses  
225 conducted during completion of this work gave, for IAEA-S1,  $\delta^{34}\text{S} = -0.378 \pm 0.17 \text{ ‰}$ ,  $\Delta^{33}\text{S} =$   
226  $0.117 \pm 0.006 \text{ ‰}$  and  $\Delta^{36}\text{S} = -0.36 \pm 0.28 \text{ ‰}$  (all  $1\sigma$ ,  $n=17$ ) and  $\delta^{34}\text{S} = 22.01 \pm 0.40 \text{ ‰}$ ,  $\Delta^{33}\text{S} =$   
227  $0.03 \pm 0.07 \text{ ‰}$  and  $\Delta^{36}\text{S} = -0.20 \pm 0.3 \text{ ‰}$  (all  $1\sigma$ ,  $n=20$ ). Those values are statistically  
228 indistinguishable from those given in Ono et al. (2006), Johnson et al. (2008) and Labidi et al.  
229 (2012). CDT samples were also analyzed. They gave raw values of  $\delta^{34}\text{S} = -0.37 \pm 0.2 \text{ ‰}$ ,  $\Delta^{33}\text{S} =$   
230  $-0.029 \pm 0.004 \text{ ‰}$  and  $\Delta^{36}\text{S} = -0.129 \pm 0.087 \text{ ‰}$  (all  $1\sigma$ ,  $n=9$ ). To express our  $\Delta^{33}\text{S}$  and  $\Delta^{36}\text{S}$   
231 results relative to V-CDT, V-CDT being assumed at zero, all results have been normalized to  
232 V-CDT using the above values and noted as  $\Delta'^{33}\text{S}$  and  $\Delta'^{36}\text{S}$ .

233 Each measurement session was preceded by a zero-enrichment. In addition, two standards  
234 (IAEA-S1, IAEA-S2 or CDT) samples were analyzed at each session, one at the beginning and  
235 one at the end to assess data quality.

236

### 237 **3. RESULTS**

238

### 239 3.1. Bulk sulfur

240

241 Our results are presented in Table 2 and Figure 1. The S isotopic composition of EH3, EH5  
242 and EL3 are all within uncertainties of each others. These values are in good agreement with  
243 Gao and Thiemens (1993a), except for the EL6 and EL7 groups, for which our values  
244 (respectively  $\delta^{34}\text{S} = -0.66 \pm 0.14 \text{ ‰}$  and  $\delta^{34}\text{S} = -0.64 \pm 0.00 \text{ ‰}$ ) are distinctively lower  
245 compared with their values ( $\delta^{34}\text{S} = -0.24 \pm 0.06 \text{ ‰}$ ,  $n = 3$ ,  $\sigma = 1$ , Gao & Thiemens, 1993a).

246

247 Aubrites (Aubrite Main Group and Shallowater) show a mean value of  $\delta^{34}\text{S} = -0.43 \pm 0.53 \text{ ‰}$   
248  $\Delta'^{33}\text{S} = 0.006 \pm 0.037 \text{ ‰}$  and  $\Delta'^{36}\text{S} = 0.041 \pm 0.237 \text{ ‰}$ . Shallowater is a particular aubrite that  
249 is thought to come from a distinct parent body (Keil 1989, 2010). As Shallowater ( $\delta^{34}\text{S} = -$   
250  $0.46 \text{ ‰}$ ) does not show any distinct isotopic composition in sulfur compared with other  
251 aubrites ( $\delta^{34}\text{S} = -0.43 \pm 0.56 \text{ ‰}$ , without Shallowater), we will not make any further  
252 distinction between the main group and Shallowater and regroup all of them in one  
253 “aubrites” entity. This merge is only made for purpose of clarity and does not imply in any  
254 way that Shallowater and the Main Group might originate from the same parent body based  
255 on S isotopic compositions.

256

257 Most of aubrites data overlap with the composition measured in enstatite chondrites, yet  
258 with several samples displaying more extreme values, between two poles, one positive ( $\delta^{34}\text{S}$   
259  $= +0.154 \text{ ‰}$  measured in Aubres) and one negative ( $\delta^{34}\text{S} = -1.350 \text{ ‰}$  as measured in  
260 Bishopville). Interestingly, Bishopville displays a significant difference in isotope composition  
261 between the two chunks (i.e. two distinct samples from two museums) that were analyzed  
262 from this meteorite ( $\delta^{34}\text{S} = -1.350 \text{ ‰}$  vs.  $\delta^{34}\text{S} = +0.215 \text{ ‰}$ ). This difference of  $1.566 \text{ ‰}$  is way

263 beyond the overall uncertainty of our analytical protocol, and must represent a sample  
264 heterogeneity. This heterogeneity is also noticeable in the different concentrations of sulfur  
265 between those two chunks, with an S content of about 1.9 wt% and 0.1 wt% for the  $^{34}\text{S}$  –  
266 depleted and –enriched samples respectively.

267

268 Cumberland Falls is a particular aubrite as it contains both clasts of aubritic nature and clasts  
269 from ordinary chondrite material that is thought to come from an impactor to the aubrite  
270 parent body. First analyses on undiscriminated powder from the meteorite gave a bulk  
271 composition of  $\delta^{34}\text{S} = -0.517 \pm 0.06 \text{ ‰}$ . Subsequent analyses on specifically selected aubritic  
272 and OC clasts showed an aubrite composition much more negative,  $\delta^{34}\text{S} = -1.903 \text{ ‰}$ , while  
273 the OC clast showed a  $\delta^{34}\text{S}$  of  $0.007 \text{ ‰}$ , in perfect agreement with an ordinary chondrite  
274 signature (Gao & Thiemens 1993a) and confirming that aubrites are also heterogeneous in S  
275 isotopes.

276

277 No obvious MIF in  $^{33}\text{S}$  or  $^{36}\text{S}$  is observed in the bulk fraction analyses (Figure 2), neither in  
278 enstatite chondrites nor aubrites, mean values of  $\Delta'^{33}\text{S}$  and  $\Delta'^{36}\text{S}$  for each group being very  
279 close to zero. There is no distinctive trend in the  $\Delta'^{33}\text{S}$  or  $\Delta'^{36}\text{S}$  individual analyses, though a  
280 slight dispersion of the values beyond the standard deviation can be noted.

281

### 282 **3.2. Water soluble fraction**

283

284 Twelve large samples (4 EH and 8 aubrites) were specifically analyzed to access the S isotope  
285 composition of oldhamite (Table 3, Figure 3). Nine of them released enough sulfur to allow  
286 for analysis of S isotopes, while three (all aubrites) did not release any significant amount of

287 sulfur. The sulfur isotopic composition of the water soluble fraction is distinctively different  
288 from the bulk S of enstatite meteorites, showing large variations between samples (with a  
289  $\delta^{34}\text{S}$  from 0.66 ‰ to 10.95 ‰) and an enrichment in all three heavy isotopes compared to  
290 bulk S compositions, with averages  $\delta^{34}\text{S} = 3.62 \pm 3.02$  ‰,  $\Delta'^{33}\text{S} = -0.024 \pm 0.027$  ‰ and  $\Delta'^{36}\text{S}$   
291  $= 0.629 \pm 0.724$  ‰. Three samples (EH3 Indarch, and aubrites Norton County and Aubres)  
292 show significant  $^{36}\text{S}$  excess (respectively  $\Delta'^{36}\text{S} = 2.23$  ‰, 1.19 ‰ and 0.91 ‰). Norton County  
293 is the only sample to show significant anomalies in both  $^{36}\text{S}$  and  $^{33}\text{S}$ , with a positive  $\Delta'^{36}\text{S}$   
294 (+1.185 ‰) and a negative anomaly in  $\Delta'^{33}\text{S}$  (-0.085 ‰). This result contrasts with the datum  
295 of Rai et al. (2005) who measured a positive anomaly in  $\Delta'^{33}\text{S}$  of  $0.161 \pm 0.012$  ‰ in  
296 oldhamite of Norton County and  $\Delta'^{36}\text{S} \approx 0$  ‰, suggesting that a given aubrite can also be  
297 isotopically heterogeneous in terms of  $^{33}\text{S}$  isotopes, best illustrated by the water soluble  
298 fraction. To our knowledge, these isotope anomalies do not compare with other data in bulk  
299 meteorites (Antonelli et al., 2014; Hulston and Thode, 1965b).

300

301

302

## 303 **4. DISCUSSION**

304

### 305 **4.1. Heterogeneity of the samples**

306

307 Previous petrographic studies have shown that at a mm scale, samples can be very  
308 heterogeneous in their mineral composition (Mason 1965, Keil 1968, Rubin 1984, Brett &  
309 Keil 1986). This is supported by S isotopes and particularly for aubrites and EL6, which  
310 contain less sulfides than the other groups. In several cases, samples from the same chunks

311 did not contain extractable sulfides. A misstep in the chemical extraction was unlikely since  
312 for samples for which enough material was available to perform replicates from the same  
313 chunk, as for pyrite tests, all the results were within experimental error. It is therefore more  
314 likely that these chunks did not contain any sulfide. Some of the samples that we had  
315 received as powders were possibly oxidized with the clear presence of rusty material.  
316 Therefore the sulfides may have been oxidized to sulfates and were not extracted by our  
317 analytical method. In order to test this possibility we performed an extraction using Thode's  
318 method (Thode et al. 1961) to extract sulfur from sulfates which did not yield anything either  
319 (see table 2). Therefore, it is more probable that the lack of sulfur was due to the  
320 heterogeneous nature of the original material (usually single chunks, or powder from a  
321 single chunk), which is expected given the brecciated nature of those samples, with clasts of  
322 mm to cm size. This idea is further supported by the fact that the two distinct chunks from  
323 Bishopville displayed contrasted isotope compositions.  
324 Although the sulfur content can be heterogeneous, the isotopic composition remains fairly  
325 reproducible between different replicates of a same meteorite with a difference of less than  
326 0.2 ‰ in  $\delta^{34}\text{S}$ , with the noticeable exceptions of Abee (EH4), which displays a variability of  
327 0.377 ‰, and Bishopville (aubrite), showing a significant variation of 1.566 ‰ in  $\delta^{34}\text{S}$ .

328

#### 329 **4.2. Mass independent isotopic fractionation in the water soluble fraction**

330

331 Significant MIF are observed in the water soluble fractions (Figure 4) of the analyzed samples  
332 showing a clear positive  $\Delta'^{36}\text{S}$  up to 2.23 ‰ for Indarch (with a corresponding  $\Delta'^{33}\text{S} = 0.006 \pm$   
333 0.01 ‰), and a slightly negative  $\Delta'^{33}\text{S}$  of -0.085 ‰ in Norton County (with a  $\Delta'^{36}\text{S} = 1.185 \pm$   
334 0.1 ‰). This contrast with the bulk sulfur fraction of EL, EH and aubrites, where very

335 restricted MIF occurs with  $-0.009\text{‰} < \Delta'^{33}\text{S} < +0.021\text{‰}$  and  $-0.160\text{‰} < \Delta'^{36}\text{S} < +0.319\text{‰}$ .  
336 Oldhamite is a rare mineral only observed naturally in enstatite meteorites (chondrites and  
337 achondrites). It has never been observed on terrestrial samples, nor in other meteorite  
338 groups. Larimer (1968) showed that this peculiarity of enstatite meteorites is probably due  
339 to a highly-reduced environment of formation, with a low oxygen fugacity ( $\log p\text{O}_2 = 8.58 -$   
340  $25.35/T$ ) associated with a high C/O ratio ( $\approx 0.9$ ).

341 If these anomalies were imputable to experimental errors, as bulk and water soluble  
342 samples were analyzed in no particular order, they would likely appear in both S fractions  
343 (bulk and water soluble) of aubrites and enstatite chondrites. However, MIF is observed only  
344 among water soluble fractions. Moreover, the samples showing MIF were not analyzed  
345 during the same sessions, therefore, it is rather unlikely that they could result from  
346 experimental errors. This MIF signal is thus real, and specific to the water soluble fraction.  
347 There are three typical explanations to generate MIF in meteorites: (1) cosmic ray spallation,  
348 including the production of cosmogenic nuclides (2) photochemically-induced gas phase  
349 chemical reactions and (3) stellar nucleosynthesis (Rai et al. 2005, Chakraborty et al. 2013,  
350 Antonelli et al. 2014).

351  
352 Spallation reactions leads to nuclides produced from interactions between highly energetic  
353 particles (cosmic rays in the case of Cosmic Ray Spallation, or CRS) and a target nuclei. CRS  
354 producing excess in S isotopes have only been studied in iron meteorites, where the target  
355 element – Fe – is the most abundant and the irradiation ages are the longest (Hulston &  
356 Thode 1965a, Hulston & Thode 1965b , Gao & Thiemens 1991). In the absence of spallation  
357 studies on enstatite meteorites, iron meteorites remain the closest analogues and a  
358 comparison with iron meteorites is supported by the fact that EH and EL are the richest



359 meteorites in iron after iron meteorites. In iron meteorites, spallation reactions is associated  
360 with a specific ratio  $\Delta^{36}\text{S}/\Delta^{33}\text{S} \approx 8$ , which does not match favorably our results in enstatite  
361 meteorites (Figure 4), making spallation an unlikely explanation for the observed MIF. In  
362 particular, spallation would only create positive  $\Delta^{33}\text{S}$  and cannot account for our slightly  
363 negative  $\Delta^{33}\text{S}$  observed in Norton County.

364

365 Ruling out cosmic ray exposure and stellar nucleosynthesis as the origin of this excess in  $^{33}\text{S}$ ,  
366 Rai et al. (2005) concluded that mass-independent induced gas phase chemical reactions in  
367 the solar nebula was more likely to explain positive  $\Delta^{33}\text{S}$  up to 0.16 ‰ in Norton County.  
368 Though our results are distinct in sign and magnitude we confirm that oldhamite, or at least,  
369 the water soluble fraction, is a carrier of MIF. The contrast of 0.25 ‰ in  $\Delta^{33}\text{S}$  between Rai et  
370 al. 2005 and this study could be the illustration of significant heterogeneity in the Norton  
371 County meteorite.

372

373 On Earth, photochemistry reactions between UV on S-atmospheric species, such as  $\text{SO}_2$ ,  
374 leads to the production of MIF (Farquhar et al. 2000a, 2001). This is a well-accepted origin  
375 for terrestrial MIF recorded in Archean sulfides and sulfates as well as present-day sulfate  
376 aerosols in Antarctic ice cores (Baroni et al. 2007, 2008). One of the solar nebula prominent  
377 species in gas phase in reducing environment nebula is  $\text{H}_2\text{S}$ . The specific isotope  
378 fractionations associated with photodissociation of  $\text{H}_2\text{S}$  are still based on a very limited set of  
379 experiments at specific wavelengths. Experiments using a wavelength of  $\sim 220$  nm show a  
380 positive  $\Delta^{36}\text{S}/\Delta^{33}\text{S}$  ratio of  $\approx +1.7$  (Farquhar et al. 2000b) while Chakraborty et al. (2013)  
381 showed that using a Lyman- $\alpha$  radiation (121.6 nm), that was suggested to be more  
382 representative of a T-Tauri sun, the  $\Delta^{36}\text{S}/\Delta^{33}\text{S}$  ratio becomes negative with a value of  $\approx -3$ .

383 Though this result supports the MIF observed in iron meteorites by Antonelli et al. (2014), it  
384 does not match our own results. It remains possible that at a particular wavelength, or a  
385 distinct spectrum that might have existed during the early stage of the Solar Nebula,  
386 photochemistry created a MIF with a much stiffer slope (a  $\Delta^{36}\text{S}/\Delta^{33}\text{S}$  ratio of  $\approx -12$  would be  
387 necessary to match our data and account for the  $\Delta^{33}\text{S}$  of  $-0.085$  ‰ measured in Norton  
388 County) but this remains to be produced by experimental data. Though the Lyman- $\alpha$  is the  
389 strongest wavelength in the nebula, a contribution of other wavelengths, others sulfide  
390 species (HS, SiS, etc...), or systems with different composition (e.g. dust/gas ratio) might lead  
391 to a distinct MIF signal. Further studies are required to help clarify these issues.

392

393 S isotope anomalies associated with nucleosynthetic sources were recently reviewed by  
394 Antonelli et al. (2014). Clayton and Ramadurai (1977) predicted an enrichment in  $^{36}\text{S}$  while  
395 enrichment in  $^{32}\text{S}$  compared to the three other S isotopes was predicted by Farquhar et al.  
396 (2000), with a slope of 1 in  $\delta^{33}\text{S}$  vs.  $\delta^{34}\text{S}$  and  $\delta^{36}\text{S}$  vs.  $\delta^{34}\text{S}$  diagrams, thus leading to a constant  
397 ratio of  $\Delta^{36}\text{S}/\Delta^{33}\text{S} \approx -1.9$ . This was later confirmed by Hoppe et al. (2012), though  $^{36}\text{S}$  was not  
398 measured. Presolar SiC grains have indeed shown depletion in  $^{33}\text{S}$  resulting in a  $\Delta^{33}\text{S}$  as low  
399 as  $-200$  ‰. Those values are thought to be inherited from S formed in the Si/S zone of SNII  
400 Supernovae (Hoppe et al. 2012). Nucleosynthetic processes in SNII supernovae could also  
401 produce enrichments in  $^{36}\text{S}$  (Woosley & Heger 2007), but those would be observed in the  
402 He/C zone and are thought to be associated with an enrichment in  $^{33}\text{S}$ , resulting in positive  
403  $\Delta^{33}\text{S}$  and  $\Delta^{36}\text{S}$ . None of these match our data, neither the bulk fraction (that shows no  
404 significant MIF, see Figure 2), nor in the water soluble fraction (Figure 4).

405

406 Antonelli et al. (2014) measured the S isotopic compositions of iron meteorite troilites. They  
407 noted slight MIF, both positive and negative ( $-0.029\text{‰} < \Delta^{33}\text{S} < +0.031\text{‰}$ ,  $-0.34\text{‰} < \Delta^{36}\text{S} <$   
408  $+0.28\text{‰}$ ), showing a weak correlation of  $\Delta^{33}\text{S}/\Delta^{36}\text{S} \approx -7$  that they interpret as being the  
409 produce of nebular photochemistry. Our data strongly overlap with those of Antonelli et al.  
410 (2014) being, therefore, consistent with such a process. However, the more restricted ranges  
411 in both  $\Delta^{33}\text{S}$  and  $\Delta^{36}\text{S}$  does not support the possibility of photochemistry-related isotope  
412 effect in our data. None of the above hypotheses gives a trend that matches the observed  
413 MIF in the water soluble fraction of the enstatite meteorite (Figure 4), and are thus unlikely  
414 explanation for our set of data.

415

416 Alternatively, the excess of  $^{36}\text{S}$  could be inherited from another water soluble phase that  
417 would contaminate the water soluble fraction during chemical extraction of the oldhamite. If  
418 a phase carrying an excess of  $^{36}\text{S}$  were to contaminate the oldhamite extract, then this  
419 excess could be misinterpreted as coming from the oldhamite itself. A possible candidate of  
420 such contamination is lawrencite ( $\text{FeCl}_2$ ). Indeed, lawrencite is water soluble and large  
421 excesses ( $> 200\text{‰}$ ) of  $\Delta^{36}\text{S}$  have been measured and have been interpreted as the result of  
422 the decay of  $^{36}\text{Cl} \rightarrow ^{36}\text{S}$  ( $\frac{1}{2}$  life  $\approx 301,000 \pm 2,000$  years) (Lin et al. 2005, Jacobsen et al. 2011).  
423  $^{36}\text{S}$  is the rarest stable isotope of sulfur ( $\sim 0.017\%$ ) and, as such, is the most sensitive to  
424 secondary isotope production.  $^{36}\text{Cl}$  ( $\frac{1}{2}$  life  $\approx 301,000 \pm 2,000$  years) decays in both  $^{36}\text{Ar}$  and  
425  $^{36}\text{S}$  ( $\sim 99$  and  $1\%$  respectively via  $^{35}\text{Cl}(n, g)^{36}\text{Cl} \rightarrow ^{36}\text{Ar}, ^{36}\text{S}$ ) and given the bearing of noble gas  
426 geochemistry to date exposure ages,  $^{36}\text{Cl}$ -production has therefore been widely studied, and  
427 is known to occur from several elements most primarily Fe, Ti, Ca and Cl (e.g. Leya et al.,  
428 2000a, 2000b).  $^{36}\text{S}$  production from  $^{36}\text{Cl}$ -decay is a viable explanation to account for the  
429 occurrence of positive  $\Delta^{36}\text{S}$  in our sample set together with a lack of  $\Delta^{33}\text{S}$ -anomaly. The only

430 exception is, again, for Norton County. Other mechanisms such as spallation reactions on Fe  
431 (see above) would indeed lead to coupled  $\Delta^{33}\text{S}$  and  $\Delta^{36}\text{S}$ -anomalies, which are not observed  
432 in our dataset. The fact that positive  $\Delta^{36}\text{S}$  are measured in two aubrites (i.e. with lower Fe-  
433 contents than enstatite chondrites) is also consistent with such an observation.

434

435 Radioactive  $^{36}\text{Cl}$  is commonly suggested to result from either nucleosynthetic anomalies (e.g.  
436 Murty et al. 1997), neutron capture reactions of Cl-rich fluid/phase for example during T-  
437 Tauri phase of the sun (Wasserburg et al. 2011, Jacobsen, 2011, Turner et al. 2013) and/or its  
438 subsequent production from primary and secondary particles on the parent body. Enstatite  
439 and aubrites have long exposure time (for review see Eugster, 2003), consistent with e.g. Sm  
440 and Gd isotopic studies (e.g. Hidaka et al., 2012).

441

442 Lawrencite ( $\text{FeCl}_2$ ) was found to bear large excesses of  $^{36}\text{S}$  ( $\Delta^{36}\text{S} > 200 \text{ ‰}$ ) which were  
443 interpreted as the result of the decay of  $^{36}\text{Cl} \rightarrow ^{36}\text{S}$  (Lin et al. 2005, Jacobsen et al. 2011).

444 Lawrencite is found in enstatite meteorites, for example it was described as an accessory  
445 mineral in the EL3 fragment of the polymict meteorite Almahata Sitta (Lin et al. 2011, Feng  
446 et al. 2012) and many other aubrites and chondrites (e.g. Lundberg et al., 1994). If produced

447 by  $^{36}\text{Cl}$ -decay produced from  $^{35}\text{Cl}$ ,  $\Delta^{36}\text{S}$  anomalies should be coupled with enrichment in both  
448  $^{36}\text{Ar}$  and  $^{38}\text{Ar}$ , the latter being produced from  $^{37}\text{Cl}(n, g)^{38}\text{Cl} \rightarrow ^{38}\text{Ar}$ . Excesses of  $^{36}\text{Ar}$  have

449 been observed in several enstatite chondrites (Okazaki et al. 2010) and aubrites (Miura et al.  
450 2006). Establishing relationships between  $^{36}\text{Ar}$  and  $^{38}\text{Ar}$  budgets remain however difficult to

451 address. The respective contribution of initial 'trapped' and produced 'cosmogenic' Ar are  
452 notably hard to calculate and is further complicated by the sensitivity of argon isotopes to

453 terrestrial weathering (Patzner and Schultz, 2001). However, we did not identify any

454 relationship between  $\Delta^{36}\text{S}$  and exposure age (see Table 2). Although the lack of relationship  
455 may be taken as an argument against  $\Delta^{36}\text{S}$  anomalies resulting from  $^{36}\text{Cl}$ -decay, it is worth  
456 noting that exposure age of aubrites (i.e. 2 of our 3 samples yielding non-zero  $\Delta^{36}\text{S}$ ) may be  
457 biased, most data being obtained on brecciated samples (Wieler, 2002; Eugster 2003, p. 11).  
458 Yet lawrencite ( $\text{FeCl}_2$ ) is a water soluble mineral and it is a likely to react and released its  
459 sulfur during the extraction of the water soluble fraction and, we suggest, is a possible  
460 candidate that should deserve future investigations. The  $^{36}\text{S}$  excess measured in the water  
461 soluble fraction does not exceed 2 ‰. Assuming that this anomaly is entirely produced by  
462 the excess of  $^{36}\text{S}$  from lawrencite and that this original excess is of  $\geq 200$  ‰, mass balance  
463 shows that less than 3 % of the  $^{36}\text{S}$  from the water soluble fraction would come from the  
464 contribution of lawrencite, which in turn represents  $\approx 0.1$  % of the total S in the samples.

465

466 It is also possible that the excess of  $\Delta^{36}\text{S}$  measured in the water soluble fraction originates  
467 from reactions with calcium, about half being likely contained in oldhamite. Few studies  
468 were devoted to the specific analysis of oldhamite; so far, no significant isotope anomaly has  
469 been recognized for Ca or S-isotopes (e.g. Lundberg et al., 1994). The errors on S-  
470 measurements (typically 2-4‰) were however too large compared with the scale of  $\Delta^{36}\text{S}$   
471 anomalies we report. Therefore, we cannot exclude that the oldhamite is not the main  
472 carrier of  $\Delta^{36}\text{S}$ -anomalies and future work on oldhamite could clarify this issue. Similarly,  
473 such investigations could help understanding the origin of the very positive  $\delta^{34}\text{S}$ -values, up  
474 to +11‰, measured in the water-soluble fraction.

475

476 The high reactivity of oldhamite and lawrencite with water could explain why it is only  
477 observed in highly reduced meteorites such as enstatite chondrites and achondrites, as the

478 slightest contact with water (aqueous alteration, weathering, sample preparation) in C and O  
479 chondrites is likely to dissolve this mineral phase and mix it with the other sulfide/sulfate  
480 pool (Larimer 1968). Moreover, if the  $^{36}\text{S}$  excess results from the decay of  $^{36}\text{Cl}$ , it will have no  
481 effect on the bulk S isotopic compositions of the samples, which is consistent with the lack of  
482 correlation between  $\Delta'^{33}\text{S}$  and  $\Delta'^{36}\text{S}$ .

483

484

### 485 **4.3. Parent Bodies**

486

487 Our data show that it is not possible to discriminate EH3, EH5 and EL3 from their isotopic  
488 composition of sulfur. Enstatite chondrites formed in an extremely reduced environment,  
489 with a  $f\text{O}_2$  as low as  $10^{-21}$  atm (800°C), significantly different from the environment of  
490 formation of ordinary and carbonaceous chondrites, that show a  $f\text{O}_2$  respectively two and  
491 three order of magnitude higher (Brett & Sato, 1983). It is possible that it is these common  
492 and peculiar conditions of formations that led to similar isotopic compositions for EL and EH  
493 parent bodies, whatever EH and EL derive or not from the same parent body. Based upon  
494 the chemical compositions of enstatite chondrites, Kallemeyn and Wasson (1986) suggested  
495 that the innermost region of the solar nebula, where enstatite meteorites most probably  
496 formed, had to be heterogeneous. Gao and Thiemens (1993a) argued against this idea,  
497 based on the evidence that EH and EL had distinct parent bodies, and yet similar S and O  
498 isotopic composition. Therefore the inner region of the nebula had to be isotopically  
499 homogeneous. However, the recent discovery of a small but significant difference between  
500 EL ( $\Delta^{17}\text{O} = -0.041 \pm 0.026 \text{ ‰}$ ) and EH ( $\Delta^{17}\text{O} = -0.066 \pm 0.027 \text{ ‰}$ ) would rather favor a slightly  
501 heterogeneous nebula (Herwartz et al. 2014). Thus, if an S isotope heterogeneity exists

502 among EH and EL, it remains within our experimental error. However, our data showing that  
503 the EL6 (average  $\delta^{34}\text{S} = -0.66 \pm 0.14 \text{ ‰}$  while average EH:  $\delta^{34}\text{S} = -0.25 \pm 0.21 \text{ ‰}$ ) might have  
504 a distinct S composition, offers two possibilities. It can either indicate heterogeneities in the  
505 isotopic composition of sulfur in the inner area of the nebula, or the parent body processes  
506 that altered the original S composition of EL6/7. Yet, a difference between the Earth's  
507 mantle and ocean of 0.1 ‰ in  $\Delta^{17}\text{O}$  (Pack and Herwartz 2013) is comparatively larger than  
508 the difference between EL and EH. If a mechanism can produce up to 0.1 ‰ on Earth, then  
509 we enter a field where a difference of 0.3 ‰ in  $\delta^{34}\text{S}$  between EL and EH may not be  
510 significant enough to highlight a nebula heterogeneity, as processes on the parent body  
511 might alternatively lead to such variability.

512

513 Even though it is generally assumed that the EH and EL groups represent only two parent  
514 bodies, some recent studies have shown remarkable differences between EL6 and other  
515 enstatite chondrites (Rubin et al. 2009, Moynier et al. 2011, Barrat et al. 2014, Wang et al.  
516 2014). In agreement with our results, showing that the sulfur isotopic ratio of EL6 is distinct  
517 from all the other enstatite chondrites, Moynier et al. (2011) have shown that the EL6 are  
518 depleted in Zn, with an estimated Zn concentration of 6 ppm (Kong et al. 1997) whereas EL3  
519 show a Zn content of 213 ppm (Kong et al. 1997) and EH chondrites show a Zn content of  
520 290 ppm (Lodders and Fegley 1998), and were also enriched in light Zn isotopes, showing a  
521  $\delta^{66}\text{Zn} = +4.88 \pm 1.79 \text{ ‰}$  ( $1\sigma$ ), compared to the other enstatite groups, both chondrites ( $\delta^{66}\text{Zn}$   
522  $= +0.25 \pm 0.16 \text{ ‰}$  ( $1\sigma$ )) and aubrites ( $\delta^{66}\text{Zn} = +4.88 \pm 1.79 \text{ ‰}$  ( $1\sigma$ )). Preferential loss of the  
523 heavier Zn isotopes would be caused by volatilization by impacts on the parent body of EL6.  
524 However, EL6 are enriched in light S isotopes, and not heavy S isotopes. Kinetically driven  
525 evaporation would enrich the residue in heavier S isotopes (e.g. Davis and Richter 2003), so

526 cannot explain the depletion in  $^{34}\text{S}$  in EL of the highest metamorphic degree. One alternative  
527 explanation could be an oxidation occurring on the EL6 parent body. McEwing et al. (1983)  
528 showed that oxidation of FeS sulfides caused enrichment in heavy S isotopes of the residue.  
529 Being the most reduced bodies, an oxidation of enstatite chondrites would lead to marked  
530 petrographic features between EL6 and other enstatite meteorites, which is however not the  
531 case, making oxidation of EL6 an unlikely explanation. Oldhamite (which can be  $^{34}\text{S}$  enriched)  
532 being one of the most refractory minerals, its preferential evaporation is also unlikely.

533

534 REE studies (Rubin et al. 2009, Barrat et al. 2014) and Fe isotopic compositions (Wang et al.  
535 2014) have also shown a unique behaviour in EL6 compared to other enstatite meteorites.  
536 Rubin et al. (2009) reported that the EL6 are depleted in siderophile and chalcophile REE and  
537 that lithophile REE are more fractionated in EL6 than in other chondrites. For instance, in EL6,  
538 the ratio  $\text{La/Yb} = 0.79$  against 1.05 for other enstatite chondrites (Rubin et al. 2009). The  
539 same goes for  $\text{Sm/Yb}$  (0.89 in EL6, 0.95 in EH),  $\text{La/Sm}$  (0.90 in EL6, 1.00 in EH) or  $\text{Ca/Sc}$  (0.86  
540 in EL6, 0.97 in EH). They have also observed a depletion in the abundance of oldhamite in  
541 EL6, which is the main carrier of the REE along with plagioclase, that can account for the REE  
542 depletion and fractionation. Wang et al. (2014) measured the isotopic compositions of Fe in  
543 all groups of enstatite meteorites and noted that, in contrast with the homogeneous  
544 compositions of EH ( $\delta^{56}\text{Fe} = 0.003 \pm 0.042 \text{ ‰}$ ) and EL3 ( $\delta^{56}\text{Fe} = 0.030 \pm 0.038 \text{ ‰}$ ), the EL6  
545 displayed a large variability in their Fe isotopic composition, showing a  $\delta^{56}\text{Fe}$  varying from -  
546 0.180 ‰ to 0.181 ‰, which they explained as the consequences of the important  
547 brecciation underwent by EL6, mixing different proportions of mineral phases with distinct  
548 Fe isotopic compositions.

549



550 The petrographic grades determined for EH meteorites range from EH3 to EH5. Though EH6  
551 do exist (Rubin & Wasson, 2011), very few have been studied. The EL group, on the other  
552 hand, shows a petrographic grade ranking up to EL6, and even EL7 for few samples. Happy  
553 Canyon is officially classified by the Meteoritical Bulletin Database as EL6/7 and Ilafegh 009 is  
554 classified as EL7. The petrographic grade of type 7 designates chondrites that have been  
555 metamorphised nearly to the point of melting. Though this term is not widely accepted, it  
556 undoubtedly indicates the highest degree of metamorphism possible for an undifferentiated  
557 body.

558

559 Thus, it is possible that the EL parent body underwent a stronger metamorphism than the EH  
560 parent body, and that this metamorphism has affected the S isotopic composition of  
561 metamorphosed material of the EL parent body while not impacting the isotopic  
562 composition of the EH parent body. Other chondritic groups do not evidence a similar  
563 difference between petrographic grades, but no study reports a complete set of  
564 petrographic grades in a particular group of meteorites and there are no high metamorphic  
565 grades in carbonaceous chondrites. However, Gao and Thiemens (1993a) measured the  
566 sulfur isotopic composition of several ordinary chondrites, including the L3 ALHA 77216 and  
567 the LL6 ALHA 83071 and no significant difference were observed compared with other OC  
568 meteorites of lower metamorphic grade.

569

570 All the compositional differences noted in EL6 compared to others enstatite meteorites can  
571 be explained by an impact-induced high metamorphism on a unique EL parent body,  
572 creating locally a volatilization of Zn (Moynier et al. 2011), a fractionation and depletion in  
573 REE (Rubin et al. 2011, Barrat et al. 2014), and the large brecciation, causing heterogeneity

574 of the Fe isotopic composition (Wang et al. 2014) as well as the loss of oldhamite that  
575 produced the light isotopic composition in S (this study).

576

#### 577 **4.4. Mass Dependent Isotopic Fractionation and loss of Oldhamite**

578

579 The variable  $\delta^{34}\text{S}$  observed in the water soluble fraction (from 0.7 ‰ up to +10.95 ‰), is  
580 distinctively different from the bulk isotopic composition that is homogeneous and slightly  
581 and consistently negative in all enstatite meteorites. There are two ways to explain the  
582 oldhamite  $^{34}\text{S}$  isotopic compositions. These positive signatures are either pristine, in which  
583 case it testifies of a different S reservoir for oldhamite than the other S-bearing minerals in  
584 the enstatite meteorites, or it has been isotopically modified and reflects an alteration  
585 process that affected only the (soluble) oldhamite. In the case of a pristine S isotopic  
586 composition, oldhamite would be the testimony of the existence of yet unknown reservoir,  
587 with the  $\Delta^{33}\text{S}$  remaining unaffected by any of the MIF-inducing processes highlighted before  
588 (spallation, UV photolysis, nucleosynthetic sources) with the possible exception of the  
589 negative  $\Delta^{33}\text{S}$  in Norton County.

590

591 Evaporation of CaS would lead to positive  $\delta^{34}\text{S}$  of residual CaS and, according to mass  
592 conservation effects (Farquhar et al., 2007) would also lead to significant but limited MIF:  
593 modelling was made using fractionation factors scaling to the square root of the mass of the  
594 evaporated species (Davies et al., 1990; Young et al., 2002) and shows that the maximum  
595  $\Delta^{33}\text{S}$  and  $\Delta^{36}\text{S}$  would be -0.04 and 0.26‰ respectively for a residual  $\delta^{34}\text{S}$  of 10 ‰. Therefore,  
596 evaporation cannot be the main process responsible for  $\Delta^{36}\text{S}$  anomalies up to +2.2‰, even if

597 we cannot rule out that it might have contributed, among other processes, to the observed  
598 isotope variability of oldhamite (or soluble fraction).

599

600 Alternatively, oldhamite is a mineral that has an extraordinary high melting temperature of  
601 about 2525°C as a pure substance (McCoy et al. 1999) but can also melt at much lower  
602 temperatures in conjunction with other phases, in particular, low  $f_{O_2}$  CaO-MgO-SiO<sub>2</sub>-CaS  
603 systems (Rudneva and Panov, 1962) and enstatite-chondrite melts (Fogel et al. 1996). Fusion  
604 experiments on Indarch have shown that at 1000°C, all sulfides and metal phases were  
605 melted (McCoy et al. 1999). This supports the idea that oldhamite should be lost through  
606 metamorphism on the EL parent body, though the occurrence of oldhamite in aubrites  
607 seems inconsistent with such an assumption.

608 It seems thus likely that a kinetic-driven alteration process could affect its S isotopic  
609 composition, leading to high <sup>34</sup>S residual compositions of the oldhamite. Figure 5 shows that  
610 apart from one anomalously CaS-rich sample (Indarch), a correlation seems to exist between  
611  $\delta^{34}\text{S}$  of the oldhamite and its proportion in sulfides. This suggests that the loss of CaS  
612 induced a concentration of heavy isotopes and thus higher  $\delta^{34}\text{S}$  in the oldhamite residue,  
613 either during impact-induced melting events on the parent body or on the Earth's surface  
614 during subsequent storage.

615

616 At equilibrium, CaS is likely to be enriched by  $\sim 0.15$  ‰ in <sup>34</sup>S, compared to FeS at  $T \approx 1200^\circ\text{C}$   
617 (as determined by extrapolating data from Ohmoto & Rye 1979; see Moretti et al. for  
618 review), while this value would rise to  $\approx 2.5$  ‰ at  $T \approx 200^\circ\text{C}$ . The loss of oldhamite is  
619 therefore consistent with a decrease of  $\delta^{34}\text{S}$  of EL6/7 but the most positive  $\delta^{34}\text{S}$  values are  
620 inconsistent with equilibrium processes and may highlight low temperature kinetic effects.

621

622 Previous studies (Rubin et al. 2009, Barrat et al. 2014) have suggested that loss of oldhamite  
623 to account for differences in REE content between EL3 and EL6. Lower REE concentrations in  
624 EL6 than in EL3 showed that REE are lost along with the oldhamite during impact-induced  
625 melting on the parent body and probably redistributed to other parts of the parent body. In  
626 every analyzed samples, the oldhamite fraction (0 to 20 % of total sulfur) shows a  
627 distinctively  $^{34}\text{S}$  enriched isotopic composition, and this  $^{34}\text{S}$  enrichment can be used to  
628 quantify this possibility. Because of the absence of EL3 fall and the most likely loss of  
629 oldhamite due to terrestrial alteration of EL3 finds and the loss of oldhamite observed in EL6  
630 it is impossible to quantify the original amount and isotopic composition of oldhamite on the  
631 EL6 parent body. However, since EH3, EH5 and aubrites do not show any systematic S  
632 isotopic variations we suggest that, despite the large variations observed of composition  
633 observed between the different groups, that they are the best available proxy to estimate  
634 the isotopic composition of the EL parent body.

635

636 In order to estimate the loss of oldhamite between EL3 and EL6, we need to estimate the  
637  $\delta^{34}\text{S}$  of the non-soluble (non-oldhamite) fraction. We make the hypothesis that the most  $^{34}\text{S}$ -  
638 depleted composition measured in an enstatite chondrite (in Pillistfer) corresponds to a  
639 100% loss of oldhamite, and therefore, a *non-soluble* value:  $\delta^{34}\text{S}_{\text{non soluble}} = -1.17 \pm 0.01 \text{ ‰}$ .  
640 Keeping in mind that Pillistfer may contain trace amounts of CaS, this value must be taken as  
641 an upper estimate of the *non-soluble* value. The mass balance for EL3 can be written:

$$642 \delta^{34}\text{S}_{\text{total}} (\text{EL3}) = X \cdot \delta^{34}\text{S}_{\text{non soluble}} + (1-X) \cdot \delta^{34}\text{S}_{\text{CaS}} \quad (3)$$

643

644 with X the fraction of non-soluble sulfides and  $\delta^{34}\text{S}_{\text{total}} (\text{EL3}) = -0.32 \pm 0.15 \text{ ‰}$ .

645

646 With Y the fraction of CaS lost, the mass balance for EL6 becomes:

647 
$$\delta^{34}\text{S}_{\text{total}} (\text{EL6}) = X \cdot \delta^{34}\text{S}_{\text{non soluble}} + (1-X)(1-Y) \cdot \delta^{34}\text{S}_{\text{CaS}} \quad (4)$$

648

649 Assuming an average difference between EL3 and EL6 of 0.3 ‰, the fraction of oldhamite  
650 lost (Y) can be deduced as a function of  $\delta^{34}\text{S}_{\text{CaS}}$  and X. We calculated X and Y for a large range  
651 of  $\delta^{34}\text{S}_{\text{CaS}}$  from 0 to 11 ‰. We found that Y is little sensitive to  $\delta^{34}\text{S}_{\text{CaS}}$  with most values  
652 between 50 and 36 % for a range of  $\delta^{34}\text{S}_{\text{CaS}}$  between 2.2 and 10.9 ‰ and corresponding X  
653 varying between 25 and 7 % respectively. This is slightly lower than Rubin et al. (2009)'s 60 %  
654 estimate of the loss of oldhamite, though remains consistent with the idea that the loss of  
655 oldhamite is linked to a difference in  $^{34}\text{S}$  between EL3 and EL6.

656

657 Therefore it does not seem necessary to invoke a distinct parent body to explain the  
658 difference of composition of EL6 compared to EL3. An advanced metamorphism, leading to  
659 the loss of oldhamite, which melts at relatively low temperatures and migrates to other  
660 regions of the parent body, can easily explain the S isotopic composition of EL6, as well as  
661 differences in composition in REE. Metamorphism and loss of oldhamite would likely be  
662 induced by impacts on the EL parent body, causing local heating, which is also supported by  
663 the loss of heavy Zn by impact-induced volatilization (Moynier et al. 2011).

664

#### 665 **4.5. The case of aubrites**

666

667 Contrary to enstatite chondrites, aubrites display a very heterogeneous sulfur isotopic  
668 composition, showing the most extremes bulk values ( $-1.350\text{‰} < \delta^{34}\text{S} < +0.154\text{‰}$ ), including

669 intermediate values overlapping the chondritic values measured in their undifferentiated  
670 counterparts. It is well accepted that the parent body of aubrites underwent local impact-  
671 induced melting events, leading, at least locally, to segregation of the molten metal and  
672 therefore partial differentiation. Segregation of metal and silicates causes a fractionation in S,  
673 enriching the silicate phase in the lighter isotopes and the metallic phase in the heavier  
674 isotopes (Shahar et al. 2009, Labidi et al. 2013). Aubrites are breccias, heavily rearranged  
675 rocks. It is therefore highly probable that the large variations in the S isotopic compositions  
676 reflect the various degrees of differentiations caused by the impact events and mixing with  
677 impact-related compounds. Even the largest samples (~1 cm<sup>3</sup>) remained relatively small  
678 compared to the coarsed brecciation of aubrite meteorites of several cm wide, and  
679 therefore were not representative of the bulk value of the meteorite samples. In particular,  
680 this likely explains the variability observed in two distinct samples of Bishopville collected  
681 from two different museum collections. In addition to the previously mentioned depletion in  
682 heavy isotopes in relation of oldhamite loss, the most negative  $\delta^{34}\text{S}$  values represents the S  
683 composition of the most differentiated fraction of silicates. All together, these processes  
684 likely explain the large S isotope variability of aubrites compared with other enstatite  
685 meteorites.

686

#### 687 **4.6. Comparison with the Earth and other meteorite groups**

688

689 Isotopic compositions of sulfur, and many other volatile and moderately-volatile elements (O,  
690 Zn...), in enstatite meteorites and Earth have emphasized a number of similarities which led  
691 to infer that they share a similar origin (Clayton et al. 1984, Javoy 1998, Javoy et al. 2010).

692 The Earth is depleted in volatile elements compared to primitive CI chondritic and enstatite

693 chondrites. It is possible that both the Earth and the Moon were essentially dry immediately  
694 after the giant impact at the origin of the Moon and that most volatiles accreted later, as a  
695 late veneer from e.g. carbonaceous chondrite or cometary-type material (Javoy 1998,  
696 Albarède et al. 2013, Paniello et al. 2013). For volatile and chalcophile/siderophile elements  
697 (Allègre et al. 1995, Malavergne et al. 2007, Dasgupta & Walker 2008, Wood and Halliday  
698 2010, Wood et al. 2010), core segregation adds an additional level of complexity.

699

700 In meteorites, sulfur is usually described as “chondritic” reflecting a limited isotope  
701 variability. The different meteorite groups and each class of meteorite greatly overlap, yet  
702 they have a rather narrow and distinct range of variation (Gao & Thiemens 1993a, Gao &  
703 Thiemens 1993b). Enstatite meteorites (average  $\delta^{34}\text{S} = -0.47 \pm 0.44 \text{‰}$  ( $1\sigma$ )) are enriched in  
704 lighter isotopes compared to both ordinary chondrites (average  $\delta^{34}\text{S} = 0.04 \pm 0.38 \text{‰}$  ( $1\sigma$ ),  
705 Gao & Thiemens 1993a) and carbonaceous chondrites. Carbonaceous chondrites display the  
706 largest range, exceeding all the measured compositions in other meteorites, with sulfides  
707 enriched in heavy isotopes (average  $\delta^{34}\text{S} = 2.02 \pm 1.01 \text{‰}$  ( $1\sigma$ ) Gao & Thiemens 1993b)  
708 compared to other meteoritic groups, while sulfates (average  $\delta^{34}\text{S} = -0.48 \pm 1.01 \text{‰}$  ( $1\sigma$ ) Gao  
709 & Thiemens 1993b) display particularly  $^{34}\text{S}$ -depleted isotope compositions, most likely  
710 representing secondary products formed during aqueous alteration of the carbonaceous  
711 chondrite parent body (Gao and Thiemens 1993b) or appeared after their fall on Earth  
712 (Gounelle & Zolenski 2001). Early studies thus suggested that the original sulfur composition  
713 of the CC parent body was actually enriched in heavy isotopes, though this has been  
714 disproved more recently by Bullock et al. (2010).

715

716 It so appears that the enstatite meteorites are the closest class of meteorites to Bulk Silicate  
717 Earth (BSE) in terms of S isotopes. Labidi et al. (2013) recently re-investigated the isotopic  
718 compositions of the convective mantle through the study of mid-ocean ridge basalts. Even  
719 though a certain variability has been observed in the isotopic composition of modern  
720 hotspots (Cabral et al. 2013), implying a variability preserved in the convective mantle, the  
721 continental crust and sediments bear reasonably little sulfur to change significantly the  
722 global budget. The convective mantle is thus representative of the BSE being comprised  
723 between -1.80 ‰ and -1.05 ‰, with an average estimate of  $-1.28 \pm 0.33$  ‰. Assuming a  
724 chondritic Earth of  $-0.02 \pm 0.06$  ‰ in  $\delta^{34}\text{S}$  (Gao and Thiemens 1993b), and about 97% of  
725 terrestrial sulfur stored in the core (Dreibus and Palme (1996), the isotope composition of  
726 BSE is compatible with a core being enriched in  $^{34}\text{S}$  compared with the residual mantle. They  
727 inferred a core-mantle isotopic fractionation factor for the  $^{34}\text{S}/^{32}\text{S}$  ratio of  $\alpha_{\text{core-mantle}} =$   
728 1.00130 (Labidi et al. 2013) compatible with the value experimentally determined by Shahar  
729 et al. (2009). This estimate is dependent on the amount of sulfur brought to Earth by late  
730 accretion events, such as the late veneer, occurring after the core segregation, which was  
731 neglected. If the little variability of “chondritic” S in meteorites (i.e. similar to OC and CC)  
732 rules out late veneer as the main contribution to the mantle, in the details, however,  
733 meteorites display a significant range of values.

734 The enrichment in light isotopes measured in EL6/7 as well as in aubrites, falls in the range  
735 of values reported by Labidi et al. (2013), suggesting that melting and differentiation could  
736 indeed lead to a silicate residual mantle depleted in  $^{34}\text{S}$ . According to models (Javoy et al.  
737 2010), since Earth accreted from enstatite-like material, a  $\delta^{34}\text{S}$ -depleted starting material  
738 can be inferred. Our data also show that the most primitive EC give an average  $\delta^{34}\text{S}$  around –  
739 0.3 ‰, which is significantly different from the  $\delta^{34}\text{S} \approx 0$  ‰ otherwise used, which therefore



740 changes the mass balance equation and requires re-estimating the amount of sulfur stored  
741 in the core. Assuming that the estimated isotopic fractionation factor remains the same  
742 ( $\alpha_{\text{core-mantle}} = 1.00130$ ), if the starting material is set at  $-0.3$  ‰, mass balance calculation  
743 shows that the amount of sulfur stored in the core drops to 75 %.

744

745

746

## 747 **5. CONCLUSION**

748

749 We measured the bulk S isotopic compositions of 33 enstatite meteorites (chondrites and  
750 aubrites) as well as the oldhamite fraction of 9 samples. As reported previously, enstatite  
751 chondrites have lighter isotopic compositions than other chondrites, displaying negative  $\delta^{34}\text{S}$   
752 in all but one samples. However, in contrast with Gao and Thiemens (1993), we showed that  
753 EL6 have a distinct S isotopic composition, even more enriched in light isotopes than all  
754 other enstatite chondrite groups. This is explained by a loss in oldhamite, which is  $^{34}\text{S}$ -  
755 enriched. Aubrites show very variable S compositions, displaying the most extreme values.  
756 This is probably due to their brecciated nature of impact-induced differentiated material  
757 and/or segregation of metal. MIF have been observed only in the oldhamite fraction and  
758 they are likely to be the product of an excess of  $^{36}\text{S}$  produced by the decay of  $^{36}\text{Cl}$  from  $\text{FeCl}_2$ ,  
759 which probably contaminated the oldhamite (water soluble) fraction during its chemical  
760 extraction. The sulfur isotopic composition measured in enstatite chondrites is distinct from  
761 the Bulk Silicate Earth, yet EL6/7 and aubrites are approaching its isotopic composition,  
762 making, in all cases, the enstatite meteorites the closest to the Earth composition, and  
763 reinforcing the idea that Earth was built from enstatite-like material.

764

765

766 **ACKNOWLEDGEMENTS**

767

768 The samples analyzed during the course of this study were kindly provided by Muséum  
769 National d'Histoire Naturelle (France), the Université Pierre et Marie Curie (France), The  
770 Smithsonian Institute (USA), The Natural History Museum of London (UK), Hawai'i Institute  
771 of Geophysics and Planetology (USA), and the NASA meteorite working group. US Antarctic  
772 meteorite samples are recovered by the Antarctic search for Meteorites (ANSMET) program  
773 which has been funded by NSF and NASA, and characterized and curated in the department  
774 of Mineral Sciences of the Smithsonian Institution and Astromaterials Curation Office at  
775 NASA Johnson Space Center. The authors thank INSU and CNES for the PNP grant. FM thanks  
776 the ERC for the Pristine Starting Grant, the Institut Universitaire de France and the ANR for a  
777 chaire de recherche IDEX SPC.

778

779

780 **REFERENCES**

781

782

- 783 Albarede, F., Ballhaus, C., Blichert-Toft, J., Lee, C.-T., Marty, B., Moynier, F., Yin, Q.-Z. (2013)  
784 Asteroidal impacts and the origin of terrestrial and lunar volatiles. *Icarus* **222**, 44–52.
- 785 Allègre, C.J., Manhès, G., Göpel, C. (1995) The age of the Earth. *Geochim. Cosmochim. Acta* **59**, 1445–  
786 1456.

787 Antonelli, M.A., Kim, S.-T., Peters, M., Labidi, J., Cartigny, P., Walker, R.J., Lyons, J.R., Hoek, J.,  
788 Farquhar, J. (2014) Early inner solar system origin for anomalous sulfur isotopes in  
789 differentiated protoplanets. *Proc. Natl. Acad. Sci.* **111**, 17749–17754.

790 Baroni, M., Savarino, J., Cole-Dai, J., Rai, V.K., Thiemens, M.H. (2008) Anomalous sulfur isotope  
791 compositions of volcanic sulfate over the last millennium in Antarctic ice cores. *J. Geophys.*  
792 *Res. Atmospheres* **113**, D20112.

793 Baroni, M., Thiemens, M.H., Delmas, R.J., Savarino, J. (2007) Mass-Independent Sulfur Isotopic  
794 Compositions in Stratospheric Volcanic Eruptions. *Science* **315**, 84–87.

795 Barrat, J.A., Zanda, B., Jambon, A., Bollinger, C. (2014) The lithophile trace elements in enstatite  
796 chondrites. *Geochim. Cosmochim. Acta* **128**, 71–94.

797 Birck, J.L., Rotaru, M., Allègre, C.J. (1999)  $^{53}\text{Mn}$ - $^{53}\text{Cr}$  evolution of the early solar system. *Geochim.*  
798 *Cosmochim. Acta* **63**, 4111–4117.

799 Brett, R., Keil, K. (1986) Enstatite chondrites and enstatite achondrites (aubrites) were not derived  
800 from the same parent body. *Earth Planet. Sci. Lett.* **81**, 1–6.

801 Brett, R., Sato, M. (1984) Intrinsic oxygen fugacity measurements on seven chondrites, a pallasite,  
802 and a tektite and the redox state of meteorite parent bodies. *Geochim. Cosmochim. Acta* **48**,  
803 111–120.

804 Bullock, E.S., McKeegan, K.D., Gounelle, M., Grady, M.M., Russell, S.S. (2010) Sulfur isotopic  
805 composition of Fe-Ni sulfide grains in CI and CM carbonaceous chondrites. *Meteorit. Planet.*  
806 *Sci.* **45**, 885–898.

807 Cabral, R.A., Jackson, M.G., Rose-Koga, E.F., Koga, K.T., Whitehouse, M.J., Antonelli, M.A., Farquhar,  
808 J., Day, J.M.D., Hauri, E.H. (2013) Anomalous sulphur isotopes in plume lavas reveal deep  
809 mantle storage of Archaean crust. *Nature* **496**, 490–493.

810 Canfield, D.E., Raiswell, R., Westrich, J.T., Reaves, C.M., Berner, R.A. (1986) The use of chromium  
811 reduction in the analysis of reduced inorganic sulfur in sediments and shales. *Chem. Geol.* **54**,  
812 149–155.

813 Cartigny, P., Boyd, S., Harris, J., Javoy, M. (1997) Nitrogen isotopes in peridotitic diamonds from  
814 Fuxian, China: the mantle signature. *Terra Nova* **9**, 175–179.

815 Casanova, I., Keil, K., Newsom, H.E. (1993) Composition of metal in aubrites: Constraints on core  
816 formation. *Geochim. Cosmochim. Acta* **57**, 675–682.

817 Chakraborty, S., Jackson, T.L., Ahmed, M., Thiemens, M.H. (2013) Sulfur isotopic fractionation in  
818 vacuum UV photodissociation of hydrogen sulfide and its potential relevance to meteorite  
819 analysis. *Proc. Natl. Acad. Sci.* **110**, 17650–17655.

820 Clayton, D.D., Ramadurai, S. (1977) On presolar meteoritic sulphides. *Nature* **265**, 427–428

821 Clayton, R.N., Mayeda, T.K. (1996) Oxygen isotope studies of achondrites. *Geochim. Cosmochim. Acta*  
822 **60**, 1999–2017.

823 Clayton, R.N., Mayeda, T.K., Rubin, A.E. (1984) Oxygen isotopic compositions of enstatite chondrites  
824 and aubrites. *J. Geophys. Res. Solid Earth* **89**, C245–C249.

825 Dasgupta, R., Walker, D. (2008) Carbon solubility in core melts in a shallow magma ocean  
826 environment and distribution of carbon between the Earth's core and the mantle. *Geochim.*  
827 *Cosmochim. Acta* **72**, 4627–4641.

828 Dauphas, N., Davis, A.M., Marty, B., Reisberg, L. (2004) The cosmic molybdenum–ruthenium isotope  
829 correlation. *Earth Planet. Sci. Lett.* **226**, 465–475.

830 Davis, A.M., Richter, F.M. (2007) Condensation and Evaporation of Solar System Materials, *Treatise*  
831 *on Geochemistry*, pp. 1–31.

832 Dreibus, G., Palme, H. (1996) Cosmochemical constraints on the sulfur content in the Earth's core.  
833 *Geochim. Cosmochim. Acta* **60**, 1125–1130.

834 El Goresy, A., Yabuki, H., Ehlers, K., Woolum, D., Pernicka, E. (1988) Qingzhen and Yamato-691: A  
835 tentative alphabet for the EH chondrites. *Antarct. Meteor. Res.* **1**, 65.

836 Eugster, O., 2003. Cosmic-ray exposure ages of meteorites and lunar rocks and their significance.  
837 *Chemie Der Erde-Geochemistry* **63**, 3-30.

838 Farquhar, J., Jackson, T.L., Thiemens, M.H. (2000a) A  $^{33}\text{S}$  enrichment in ureilite meteorites: evidence  
839 for a nebular sulfur component. *Geochim. Cosmochim. Acta* **64**, 1819–1825.

840 Farquhar, J., Savarino, J., Jackson, T.L., Thiemens, M.H. (2000b) Evidence of atmospheric sulphur in  
841 the martian regolith from sulphur isotopes in meteorites. *Nature* **404**, 50–52.

842 Farquhar, J., Savarino, J., Airieau, S., Thiemens, M.H. (2001) Observation of wavelength-sensitive  
843 mass-independent sulfur isotope effects during  $\text{SO}_2$  photolysis: Implications for the early  
844 atmosphere. *J. Geophys. Res. Planets* **106**, 32829–32839.

845 Feng, L., Elgoresy, A., Zhang, J., Hao, J., Boyet, M., Yang, L. (2012) Excess  $^{36}\text{S}$  in Lawrencite and  
846 Nitrogen Isotopic Compositions of Sinoite from Almahata Sitta MS-17 EL3 Chondrite  
847 Fragment. *Lunar and Planetary Science Conference*, p. 1766.

848 Fitoussi, C., Bourdon, B. (2012) Silicon Isotope Evidence Against an Enstatite Chondrite Earth. *Science*  
849 **335**, 1477–1480.

850 Gao, X., Thiemens, M.H. (1991) Systematic study of sulfur isotopic composition in iron meteorites  
851 and the occurrence of excess  $^{33}\text{S}$  and  $^{36}\text{S}$ . *Geochim. Cosmochim. Acta* **55**, 2671–2679.

852 Gao, X., Thiemens, M.H. (1993a) Variations of the isotopic composition of sulfur in enstatite and  
853 ordinary chondrites. *Geochim. Cosmochim. Acta* **57**, 3171–3176.

854 Gao, X., Thiemens, M.H. (1993b) Isotopic composition and concentration of sulfur in carbonaceous  
855 chondrites. *Geochim. Cosmochim. Acta* **57**, 3159–3169.

856 Gounelle, M., Zolensky, M.E. (2001) A terrestrial origin for sulfate veins in CI1 chondrites. *Meteorit.*  
857 *Planet. Sci.* **36**, 1321–1329.

858 Herwartz, D., Pack, A., Friedrichs, B., Bischoff, A. (2014) Identification of the giant impactor Theia in  
859 lunar rocks. *Science* **344**, 1146–1150.

860 Hidaka, H., Kondo, T., and Yoneda, S., 2012. Heterogeneous isotopic anomalies of Sm and Gd in the  
861 Norton County meteorite: evidence for irradiation from the active early sun. *Astrophysical*  
862 *Journal* **746**.

863 Hoppe, P., Fujiya, W., Zinner, E. (2012) Sulfur Molecule Chemistry in Supernova Ejecta Recorded by  
864 Silicon Carbide Stardust. *Astrophys. J. Lett.* **745**, L26.

865 Hulston, J.R., Thode, H.G. (1965a) Cosmic-ray-produced S36 and S33 in the metallic phase of iron  
866 meteorites. *J. Geophys. Res.* **70**, 4435–4442.

867 Hulston, J.R., Thode, H.G. (1965b) Variations in the <sup>33</sup>S, <sup>34</sup>S, and <sup>36</sup>S contents of meteorites and their  
868 relation to chemical and nuclear effects. *J. Geophys. Res.* **70**, 3475–3484.

869 Jacobsen, B., Matzel, J., Hutcheon, I.D., Krot, A.N., Yin, Q.-Z., Nagashima, K., Ramon, E.C., Weber, P.K.,  
870 Ishii, H.A., Ciesla, F.J. (2011) Formation of the short-lived radionuclide <sup>36</sup>Cl in the  
871 protoplanetary disk during late-stage irradiation of a volatile-rich reservoir. *Astrophys. J. Lett.*  
872 **731**, L28.

873 Javoy, M. (1998) The birth of the Earth's atmosphere: the behaviour and fate of its major elements.  
874 *Chem. Geol.* **147**, 11–25.

875 Javoy, M., Kaminski, E., Guyot, F., Andrault, D., Sanloup, C., Moreira, M., Labrosse, S., Jambon, A.,  
876 Agrinier, P., Davaille, A., others( 2010) The chemical composition of the Earth: Enstatite  
877 chondrite models. *Earth Planet. Sci. Lett.* **293**, 259–268.

878 Javoy, M., Pineau, F. (1983) Stable isotope constraints on a model Earth from a study of mantle  
879 nitrogen. *Meteoritics* **18**, 320.

880 Johnston, D.T., Farquhar, J., Habicht, K.S., Canfield, D.E. (2008) Sulphur isotopes and the search for  
881 life: strategies for identifying sulphur metabolisms in the rock record and beyond. *Geobiology*  
882 **6**, 425–435.

883 Kallemeyn, G.W., Wasson, J.T. (1986) Compositions of enstatite (EH3, EH4,5 and EL6) chondrites:  
884 Implications regarding their formation. *Geochim. Cosmochim. Acta* **50**, 2153–2164.

885 Keil, K. (1968) Mineralogical and chemical relationships among enstatite chondrites. *J. Geophys. Res.*  
886 **73**, 6945–6976.

887 Keil, K. (2010) Enstatite achondrite meteorites (aubrites) and the histories of their asteroidal parent  
888 bodies. *Chem. Erde - Geochem.* **70**, 295–317.

889 Kong, P., Mori, T., Ebihara, M. (1997) Compositional continuity of enstatite chondrites and  
890 implications for heterogeneous accretion of the enstatite chondrite parent body. *Geochim.*  
891 *Cosmochim. Acta* **61**, 4895–4914.

892 Labidi, J., Cartigny, P., Birck, J.L., Assayag, N., Bourrand, J.J. (2012) Determination of multiple sulfur  
893 isotopes in glasses: A reappraisal of the MORB  $\delta^{34}\text{S}$ . *Chem. Geol.* **334**, 189–198.

894 Labidi, J., Cartigny, P., Moreira, M. (2013) Non-chondritic sulphur isotope composition of the  
895 terrestrial mantle. *Nature* **501**, 208–211.

896 Larimer, J.W. (1968) An experimental investigation of oldhamite, CaS; and the petrologic significance  
897 of oldhamite in meteorites. *Geochim. Cosmochim. Acta* **32**, 965–982.

898 Leya, I., Lange, H. J., Lupke, M., Neupert, U., Daunke, R., Fanenbruck, O., Michel, R., Rosel, R.,  
899 Meltzow, B., Schiekkel, T., Sudbrock, F., Herpers, U., Filges, D., Bonani, G., Dittrich-Hannen, B.,  
900 Suter, M., Kubik, P. W., and Synal, H. A., 2000a. Simulation of the interaction of galactic  
901 cosmic-ray protons with meteoroids: On the production of radionuclides in thick gabbro and  
902 iron targets irradiated isotropically with 1.6 GeV protons. *Meteoritics & Planetary Science* **35**,  
903 287-318.

904 Leya, I., Lange, H. J., Neumann, S., Wieler, R., and Michel, R., 2000b. The production of cosmogenic  
905 nuclides in stony meteoroids by galactic cosmic-ray particles. *Meteoritics & Planetary Science*  
906 **35**, 259-286.

907 Leya, I. and Masarik, J., 2009. Cosmogenic nuclides in stony meteorites revisited. *Meteoritics &*  
908 *Planetary Science* **44**, 1061-1086.

909 Lin, Y., El Goresy, A. (2002) A comparative study of opaque phases in Qingzhen (EH3) and MacAlpine  
910 Hills 88136 (EL3): Representatives of EH and EL parent bodies. *Meteorit. Planet. Sci.* **37**, 577–  
911 599.

912 Lin, Y., Guan, Y., Leshin, L.A., Ouyang, Z., Wang, D. (2005) Short-lived chlorine-36 in a Ca- and Al-rich  
913 inclusion from the Ningqiang carbonaceous chondrite. *Proc. Natl. Acad. Sci.* **102**, 1306–1311.

- 914 Lin, Y., El Goresy, A., Boyet, M., Feng, L., Zhang, J., Hao, J. (2011) Earliest solid condensates consisting  
915 of the assemblage oldhamite, sinoite, graphite and excess  $^{36}\text{S}$  in lawrencite from Almahata  
916 Sitta MS-17 EL3 Chondrite Fragment, *Workshop on Formation of the First Solids in the Solar*  
917 *System*.
- 918 Lodders, K., Fegley, B. (1998) The planetary scientist's companion. *Oxford University Press*.
- 919 Lorenzetti, S., Eugster, O., Busemann, H., Marti, K., Burbine, T.H., McCoy, T. (2003) History and origin  
920 of aubrites. *Geochim. Cosmochim. Acta* **67**, 557–571.
- 921 Lundberg, L. L., Zinner, E., and Crozaz, G., 1994. Search for isotopic anomalies in oldhamite (CaS) from  
922 unequilibrated (E3) enstatite chondrites. *Meteoritics* **29**, 384-393.
- 923 Malavergne, V., Tarrida, M., Combes, R., Bureau, H., Jones, J., Schwandt, C. (2007) New high-pressure  
924 and high-temperature metal/silicate partitioning of U and Pb: Implications for the cores of  
925 the Earth and Mars. *Geochim. Cosmochim. Acta* **71**, 2637–2655.
- 926 Marini, L., Moretti, R., Accornero, M. (2011) Sulfur Isotopes in Magmatic-Hydrothermal Systems,  
927 Melts, and Magmas. *Rev. Mineral. Geochem.* **73**, 423–492.
- 928 Mason, B. (1966) The enstatite chondrites. *Geochim. Cosmochim. Acta* **30**, 23–39.
- 929 McCoy, T.J., Dickinson, T.L., Lofgren, G.E. (1999) Partial melting of the Indarch (EH4) meteorite: A  
930 textural, chemical, and phase relations view of melting and melt migration. *Meteorit. Planet.*  
931 *Sci.* **34**, 735–746.
- 932 McEwing, C. e., Rees, C. e., Thode, H. g. (1983) Sulphur Isotope Ratios in the Canyon Diablo Metallic  
933 Spheroids. *Meteoritics* **18**, 171–178.
- 934 Miura, Y.N., Hidaka, H., Nishiizumi, K., Kusakabe, M. (2007) Noble gas and oxygen isotope studies of  
935 aubrites: A clue to origin and histories. *Geochim. Cosmochim. Acta* **71**, 251–270.
- 936 Moynier, F., Agranier, A., Hezel, D.C., Bouvier, A. (2010) Sr stable isotope composition of Earth, the  
937 Moon, Mars, Vesta and meteorites. *Earth Planet. Sci. Lett.* **300**, 359–366.



938 Moynier, F., Day, J.M.D., Okui, W., Yokoyama, T., Bouvier, A., Walker, R.J., Podosek, F.A. (2012)  
939 Planetary-Scale Strontium Isotopic Heterogeneity and the Age of Volatile Depletion of Early  
940 Solar System Materials. *Astrophys. J.* **758**, 45.

941 Moynier, F., Paniello, R.C., Gounelle, M., Albarède, F., Beck, P., Podosek, F., Zanda, B. (2011) Nature  
942 of volatile depletion and genetic relationships in enstatite chondrites and aubrites inferred  
943 from Zn isotopes. *Geochim. Cosmochim. Acta* **75**, 297–307.

944 Newton, J., Franchi, I.A., Pillinger, C.T. (2000) The oxygen-isotopic record in enstatite meteorites.  
945 *Meteorit. Planet. Sci.* **35**, 689–698.

946 Ohmoto, H., Rye, R. (1979) Isotopes of sulfur and carbon. *Geochem. Hydrothermal Ore Depos. Ed*  
947 509–567.

948 Okazaki, R., Takaoka, N., Nagao, K., Nakamura, T., 2010. Noble gases in enstatite chondrites released  
949 by stepped crushing and heating. *Meteorit. Planet. Sci.* **45**, 339–360.

950 Ono, S., Wing, B., Johnston, D., Farquhar, J., Rumble, D. (2006) Mass-dependent fractionation of  
951 quadruple stable sulfur isotope system as a new tracer of sulfur biogeochemical cycles.  
952 *Geochim. Cosmochim. Acta* **70**, 2238–2252.

953 Paniello, R.C., Day, J.M.D., Moynier, F. (2012) Zinc isotopic evidence for the origin of the Moon.  
954 *Nature* **490**, 376–379.

955 Patzer, A., Schultz, L. (2001) Noble gases in enstatite chondrites I: Exposure ages, pairing, and  
956 weathering effects. *Meteorit. Planet. Sci.* **36**, 947–961.

957 Quirico, E., Bourot-denise, M., Robin, C., Montagnac, G., Beck, P. (2011) A reappraisal of the  
958 metamorphic history of EH3 and EL3 enstatite chondrites. *Geochim. Cosmochim. Acta* **75**,  
959 3088–3102.

960 Rai, V.K., Jackson, T.L., Thiemens, M.H. (2005) Photochemical mass-independent sulfur isotopes in  
961 achondritic meteorites. *Science* **309**, 1062–1065.

- 962 Robinson, B. W. (1995). Sulphur isotope standards. *Reference and intercomparison materials for*  
963 *stable isotopes of light elements. IAEA-TECDOC-825. International Atomic Energy Agency,*  
964 *Vienna, 39K-45.*
- 965 Rubin, A.E. (1984) The Blithfield meteorite and the origin of sulfide-rich, metal-poor clasts and  
966 inclusions in brecciated enstatite chondrites. *Earth Planet. Sci. Lett.* **67**, 273–283.
- 967 Rubin, A.E., Huber, H., Wasson, J.T. (2009) Possible impact-induced refractory-lithophile  
968 fractionations in EL chondrites. *Geochim. Cosmochim. Acta* **73**, 1523–1537.
- 969 Rubin, A.E., Wasson, J.T. (2011) Shock effects in “EH6” enstatite chondrites and implications for  
970 collisional heating of the EH and EL parent asteroids. *Geochim. Cosmochim. Acta* **75**, 3757–  
971 3780.
- 972 Rudneva, A.V., Panov, A.S. (1962) The effect of calcium sulfide on the phase composition of slags in  
973 the system CaO-MgO-SiO<sub>2</sub>. *Bull. Acad. Sci. USSR Div. Chem. Sci.* **11**, 510–513.
- 974 Sanloup, C., Jambon, A., Gillet, P. (1999) A simple chondritic model of Mars. *Phys. Earth Planet. Inter.*  
975 **112**, 43–54.
- 976 Savage, P.S., Moynier, F. (2013) Silicon isotopic variation in enstatite meteorites: Clues to their origin  
977 and Earth-forming material. *Earth Planet. Sci. Lett.* **361**, 487–496.
- 978 Sears, D.W. (1980) Formation of E chondrites and aubrites—A thermodynamic model. *Icarus* **43**,  
979 184–202.
- 980 Shahar, A., Fei, Y., Liu, M.C., Wang, J. (2009) Sulfur isotopic fractionation during the differentiation of  
981 Mars. *Geochim. Cosmochim. Acta Suppl.* **73**, 1201.
- 982 Simon, J.I., DePaolo, D.J. (2010) Stable calcium isotopic composition of meteorites and rocky planets.  
983 *Earth Planet. Sci. Lett.* **289**, 457–466.
- 984 Thode, H.G., Monster, J., Dunford, H.B. (1961) Sulphur isotope geochemistry. *Geochim. Cosmochim.*  
985 *Acta* **25**, 159–174.
- 986 Trinquier, A., Birck, J.-L., Allègre, C.J. (2007a) Widespread <sup>54</sup>Cr Heterogeneity in the Inner Solar  
987 System. *Astrophys. J.* **655**, 1179.

988 Trinquier, A., Bizzarro, M., Ulfbeck, D. (2007b) 50 Ti anomalies in primitive and differentiated  
989 meteorites. *Geochim Cosmochim Acta* **71**, A1038.

990 Trinquier, A., Elliott, T., Ulfbeck, D., Coath, C., Krot, A.N., Bizzarro, M. (2009) Origin of  
991 Nucleosynthetic Isotope Heterogeneity in the Solar Protoplanetary Disk. *Science* **324**, 374–  
992 376.

993 Turner, G., Crowther, S.A., Burgess, R., Gilmour, J.D., Kelley, S.P., Wasserburg, G.J. (2013) Short lived  
994 <sup>36</sup>Cl and its decay products <sup>36</sup>Ar and <sup>36</sup>S in the early solar system. *Geochim. Cosmochim.*  
995 *Acta* **123**, 358–367.

996 Valdes, M.C., Moreira, M., Foriel, J., Moynier, F. (2014) The nature of Earth's building blocks as  
997 revealed by calcium isotopes. *Earth Planet. Sci. Lett.* **394**, 135–145.

998 Wang, K., Savage, P.S., Moynier, F. (2014) The iron isotope composition of enstatite meteorites:  
999 Implications for their origin and the metal/sulfide Fe isotopic fractionation factor. *Geochim.*  
1000 *Cosmochim. Acta* **142**, 149–165.

1001 Wasserburg, G.J., Hutcheon, I.D., Aléon, J., Ramon, E.C., Krot, A.N., Nagashima, K., Brearley, A.J.  
1002 (2011) Extremely Na- and Cl-rich chondrule from the CV3 carbonaceous chondrite Allende.  
1003 *Geochim. Cosmochim. Acta* **75**, 4752–4770.

1004 Watters, T.R., Prinz, M. (1979) Aubrites-Their origin and relationship to enstatite chondrites, *Lunar*  
1005 *and Planetary Science Conference Proceedings*. pp. 1073–1093.

1006 Weisberg, M.K., Kimura, M. (2012) The unequilibrated enstatite chondrites. *Chem. Erde-Geochem.* **72**,  
1007 2, 101-115.

1008 Wieler, R., 2002. Cosmic-ray-produced noble gases in meteorites, *Noble Gases in Geochemistry and*  
1009 *Cosmochemistry*. Rev. Mineral. Geo. **47**, 125-170.

1010 Wood, B.J., Halliday, A.N. (2010) The lead isotopic age of the Earth can be explained by core  
1011 formation alone. *Nature* **465**, 767–770.

1012 Wood, B.J., Halliday, A.N., Rehkämper, M. (2010) Volatile accretion history of the Earth. *Nature* **467**,  
1013 E6–E7.

1014 Woosley, S.E., Heger, A. (2007) Nucleosynthesis and remnants in massive stars of solar metallicity.  
1015 *Phys. Rep.* **442**, 269–283.

1016 Zhang, J., Dauphas, N., Davis, A.M., Leya, I., Fedkin, A. (2012) The proto-Earth as a significant source  
1017 of lunar material. *Nat. Geosci.* **5**, 251–255.

1018 Zhang, Y., Benoit, P.H., Sears, D.W.G. (1995) The classification and complex thermal history of the  
1019 enstatite chondrites. *J. Geophys. Res. Planets* **100**, 9417–9438.

1020

1021

1022

## 1023 LEGENDS

1024

1025 Table 1: Averages of S isotopic analyses of standards Canyon Diablo Troilite (CDT), IAEA-S1  
1026 and IAEA-S2.  $\delta^{34}\text{S}$  is expressed vs. V-CDT,  $\Delta^{33}\text{S}$  and  $\Delta^{36}\text{S}$  are expressed vs. our SF6 tank.  
1027  $\Delta'^{33}\text{S}$  and  $\Delta'^{36}\text{S}$  are corrected values expressed vs. V-CDT. Standard deviations are  
1028 given in  $1\sigma$ .

1029

1030 Table 2: Sulfur and oxygen isotopic compositions of bulk fraction of enstatite chondrites and  
1031 aubrites.  $\delta^{34}\text{S}$  is expressed vs. V-CDT,  $\Delta'^{33}\text{S}$  and  $\Delta'^{36}\text{S}$  are corrected values expressed  
1032 vs. V-CDT. Individual analysis precision are standard deviation of 0.01 ‰ on  $\delta^{33}\text{S}$  and  
1033  $\delta^{34}\text{S}$  and 0.1 ‰ on  $\delta^{36}\text{S}$  ( $1\sigma$ ).

1034

1035 Table 3: Sulfur isotopic composition of the water soluble fraction of enstatite chondrites and  
1036 aubrites.  $\delta^{34}\text{S}$  is expressed vs. V-CDT,  $\Delta'^{33}\text{S}$  and  $\Delta'^{36}\text{S}$  are corrected values expressed  
1037 vs. V-CDT. Individual analysis precision are standard deviation of 0.01 ‰ on  $\delta^{33}\text{S}$  and  
1038  $\delta^{34}\text{S}$  and 0.1 ‰ on  $\delta^{36}\text{S}$  ( $1\sigma$ ).

1039

1040 Figure 1: Sulfur isotopic composition in the different groups of enstatite chondrites and  
1041 aubrites.  $\delta'^{34}\text{S} = 1000 \times \ln(\delta^{34}\text{S}/1000+1)$ ,  $\delta'^{33}\text{S} = 1000 \times \ln(\delta^{33}\text{S}/1000+1)$ .  $\Delta'^{33}\text{S}$  and  $\Delta'^{36}\text{S}$   
1042 are corrected values expressed vs. V-CDT

1043

1044 Figure 2:  $\Delta'^{33}\text{S}$  and  $\Delta'^{36}\text{S}$  compositions in the different groups of enstatite chondrites and  
1045 aubrites.  $\Delta'^{33}\text{S}$  and  $\Delta'^{36}\text{S}$  are corrected values expressed vs. V-CDT.

1046

1047 Figure 3: Sulfur isotopic composition of the water soluble fraction in enstatite chondrites and  
1048 aubrites.  $\delta'^{34}\text{S} = 1000 \times \ln(\delta^{34}\text{S}/1000 + 1)$ ,  $\delta'^{33}\text{S} = 1000 \times \ln(\delta^{33}\text{S}/1000 + 1)$

1049

1050 Figure 4:  $\Delta'^{33}\text{S}$  and  $\Delta'^{36}\text{S}$  compositions in the water soluble fraction of enstatite chondrites  
1051 and aubrites. Spallation trend defined by Antonelli et al. (2014). Nebular trend  
1052 defined by Farquhar et al. (2000). Photochemical trend defined by Chakraborty  
1053 (2013).  $\Delta'^{33}\text{S}$  and  $\Delta'^{36}\text{S}$  are corrected values expressed vs. V-CDT.

1054

1055 Figure 5: Relation between  $\delta^{34}\text{S}$  composition of the water soluble fraction and the  
1056 concentration in CaS in enstatite meteorites.  $\delta'^{34}\text{S} = 1000 \times \ln(\delta^{34}\text{S}/1000 + 1)$ .

1057

1058 Appendix A: Replicate analyses of S isotopic analyses of standards Canyon Diablo Troilite  
1059 (CDT), IAEA-S1 and IAEA-S2.  $\delta^{34}\text{S}$  is expressed vs. V-CDT,  $\Delta^{33}\text{S}$  and  $\Delta^{36}\text{S}$  are expressed  
1060 vs. our SF6 tank.  $\Delta'^{33}\text{S}$  and  $\Delta'^{36}\text{S}$  are corrected values expressed vs. V-CDT. Individual  
1061 analysis precision are of 0.01 ‰ on  $\delta^{33}\text{S}$  and  $\delta^{34}\text{S}$  and 0.1 ‰ on  $\delta^{36}\text{S}$  (1 $\sigma$ ).

1062

Table 1

Sample	$\delta^{34}\text{S}$ (‰)	$\Delta^{33}\text{S}$ (‰)	$\Delta^{36}\text{S}$ (‰)	$\Delta^{33}\text{S}$ (‰)	$\Delta^{36}\text{S}$ (‰)
CDT (average)	<b>-0.377</b>	<b>-0.029</b>	<b>-0.129</b>	<b>0.000</b>	<b>0.000</b>
std. dev.	0.210	0.005	0.087	0.005	0.087
IAEA-1 (average)	<b>-0.296</b>	<b>0.088</b>	<b>-0.486</b>	<b>0.117</b>	<b>-0.357</b>
std. dev.	0.168	0.006	0.274	0.006	0.274
IAEA-2 (average)	<b>22.091</b>	<b>0.030</b>	<b>-0.197</b>	<b>0.059</b>	<b>-0.068</b>
std. dev.	0.395	0.075	0.298	0.075	0.298
IAEA-3 (average)	<b>-32.510</b>	<b>0.070</b>	<b>-0.501</b>	<b>0.099</b>	<b>-0.372</b>
std. dev.	0.063	0.007	0.260	0.007	0.260

Table 2

Sample	group	replica	std dev. on replica (1σ)			std dev. on replica (1σ)			[S] (wt%)	std dev. on replica (1σ)	δ17O (‰) δ18O (‰) Δ17O (‰)			Exposure age based on H3 composition (Ma)		
			δ34S (‰)	Δ33S (‰)	Δ36S (‰)	δ17O (‰)	δ18O (‰)	Δ17O (‰)								
Sahara 97096	EH3	2	-0.136	0.252	-0.003	0.001	0.009	0.042	4.4	0.51	2.77	5.45	-0.07	(a)	9.00	(d)
Kota-Kota	EH3	2	-0.251	0.166	0.000	0.002	0.282	0.146	3.6	0.09	2.52	5.12	-0.15	(a)	36.50	(d)
Alha 77295	EH3	3	-0.312	0.289	-0.007	0.005	0.042	0.062	4.3	0.13	--	--	--			
Mil 07028	EH3	2	-0.400	0.096	0.007	0.001	-0.049	0.046	5.4	0.31	2.39	4.54	-0.04	(c)		
Gro 95517	EH3	5	-0.192	0.169	0.000	0.004	0.292	0.062	4.0	0.18	1.84	3.55	-0.02	(c)	35.10	(d)
Qingzhen	EH4	1	0.150	--	0.000	--	0.116	--	4.1	--	2.83	5.52	-0.04	(b)	1.90	(d)
Abee	EH4	6	-0.672	0.289	0.003	0.009	0.143	0.059	4.5	0.86	3.47	6.32	0.19	(a)	7.70	(d)
Indarch	EH4	3	-0.429	0.140	-0.002	0.006	-0.037	0.046	3.6	0.81	--	--	--		8.20	(d)
St. Mark's	EH5	5	-0.381	0.120	0.002	0.005	0.056	0.108	3.3	0.90	3.15	5.73	0.18	(a)	0.68	(d)
Saint-Sauveur	EH5	4	-0.025	0.055	0.004	0.002	0.027	0.006	5.2	0.27	--	--	--			
LAP 02 225	EH5	3	-0.062	0.197	0.004	0.004	0.008	0.007	2.4	0.31	--	--	--			
Itqiy	EH7-an	3	--	--	--	--	--	--	0.0	--	--	--	--			
MAC 88136	EL3	3	-0.469	0.097	0.007	0.003	0.009	0.037	2.2	0.06	2.01	4.07	-0.11	(b)	1.20	(d)
MAC 02837	EL3	3	-0.165	0.090	0.004	0.004	0.059	0.015	2.8	0.23	1.96	3.84	0.11	(c)		
Hvittis	EL6	2	-0.455	0.089	0.000	0.016	-0.160	0.087	2.4	0.33	3.02	5.68	0.07	(a)	18.90	(d)
Khairpur	EL6	1	-0.543	--	0.010	--	0.071	--	3.3	--	3.17	6.09	0.01	(b)		
Eagle	EL6	4	-0.642	0.211	0.008	0.006	-0.009	0.071	2.0	0.60	2.79	5.44	0.03	(c)	29.40	(d)
LON 94100	EL6	1	-0.721	--	-0.001	--	0.111	--	1.6	--	--	--	--		32.60	(d)
Pillistfer	EL6	1	-1.017	--	-0.007	--	-0.139	--	1.1	--	2.92	5.58	0.02	(a)	4.10	(d)
Atlanta	EL6	1	-0.521	--	0.008	--	0.024	--	2.3	--	2.96	5.63	0.03	(a)	32.30	(d)
Blithfield	EL6	1	-0.644	--	0.008	--	-0.035	--	4.9	--	2.82	5.29	0.07	(a)		
EET 92063	EL6	3	-0.655	0.262	-0.002	0.005	-0.024	0.037	1.8	0.14	3.06	5.84	0.03	(b)	35.30	(d)
NWA 974	EL6	3	-0.801	0.173	0.008	0.003	0.269	0.041	2.0	0.57	3.32	5.94	0.22	(c)		
North West Forest	EL6	1	--	--	--	--	--	--	0.0	--	--	--	--			
Happy Canyon	EL7	1	-0.637	--	-0.009	--	0.070	--	0.2	0.07	--	--	--		26.80	(d)
Ilafegh	EL7	3	-0.638	0.564	0.001	0.006	-0.085	0.015	0.5	0.22	--	--	--		3.80	(d)
Shallowater	Aubrites	1	-0.465	--	0.008	--	0.319	--	2.8	--	2.99	5.79	-0.02	(b)	0.28	(f)
Bishopville	Aubrites	1	-1.350	0.783	0.021	0.010	0.094	0.011	1.0	0.88	2.59	5.09	0.09	(b)	52.5	(f)
Bishopville	Aubrites	1	0.215	--	0.000	--	0.117	--	--	--	--	--	--			
Norton County	Aubrites	1	-1.150	--	-0.008	--	0.023	--	0.6	0.13	2.57	4.98	-0.02	(b)	117.4	(f)
Aubres	Aubrites	1	0.451	--	-0.003	--	-0.027	--	0.3	--	--	--	--			
Bustee	Aubrites	4	-0.189	0.080	0.008	0.001	-0.006	0.040	0.1	0.01	--	--	--		50.8	(f)
Khor Temiki	Aubrites	1	-0.154	--	0.013	--	0.020	--	0.3	--	--	--	--		53.9	(f)
Mayo Belwa	Aubrites	1	-0.404	--	0.007	--	-0.083	--	0.2	--	--	--	--		102.4	(f)
Pena Blanca Spring	Aubrites	1	-0.766	--	0.008	--	-0.033	--	--	--	--	--	--		69.5	(f)
Cumberland Falls	Aubrites	2	-0.517	0.068	0.011	0.003	-0.015	0.014	1.5	0.95	3.36	5.44	0.53	(b)		
Cumber. (Aubrite clast)	Aubrites	1	-1.903	--	0.017	--	0.078	--	0.1	--	--	--	--			
Cumber. (chondrite clast)	Aubrites	1	0.007	--	0.006	--	0.089	--	0.9	--	--	--	--			

(a) Clayton et al. 1884 (b) Newton et al. 2000 (c) this study (d) Patzer &amp; Schultz 2001 (f) Lorenzetti 2003

**Table 3**

Sample	group	replica	$\delta^{34}\text{S}$ (‰)	$\Delta^{33}\text{S}$ (‰)	$\Delta^{36}\text{S}$ (‰)	%CaS in S (wt%)
Abee	EH3/4	1	2.477	-0.015	0.061	3.1
Indarch	EH3/4	1	4.503	0.006	2.229	0.1
St Mark's	EH5	1	0.666	-0.004	0.058	9.3
St Sauveur	EH5	1	0.903	-0.003	0.178	4.8
Aubres	Aubrites	1	2.219	-0.025	0.906	0.7
Bustee	Aubrites	1	4.149	-0.037	0.065	61.9
Mayo Belwa	Aubrites	1	5.370	-0.028	0.348	3.5
Norton County	Aubrites	1	10.946	-0.085	1.185	1.2
Pena Blanca Spring	Aubrites	1	1.324	0.011	-0.048	--
Cumberland Falls	Aubrites	1	--	--	--	0.0
Bishopville	Aubrites	1	--	--	--	0.0
Khor Temiki	Aubrites	1	--	--	--	0.0



Figure 1

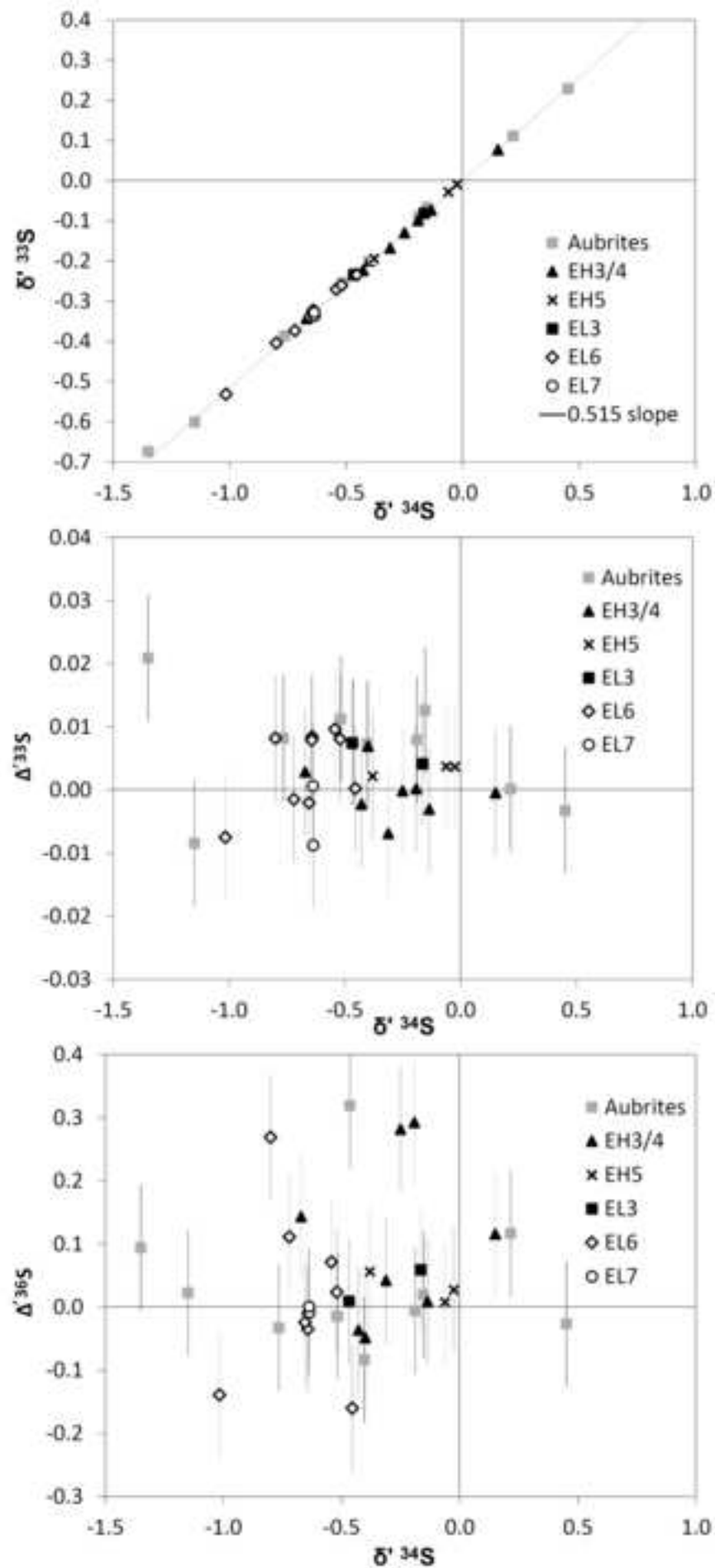




Figure 4

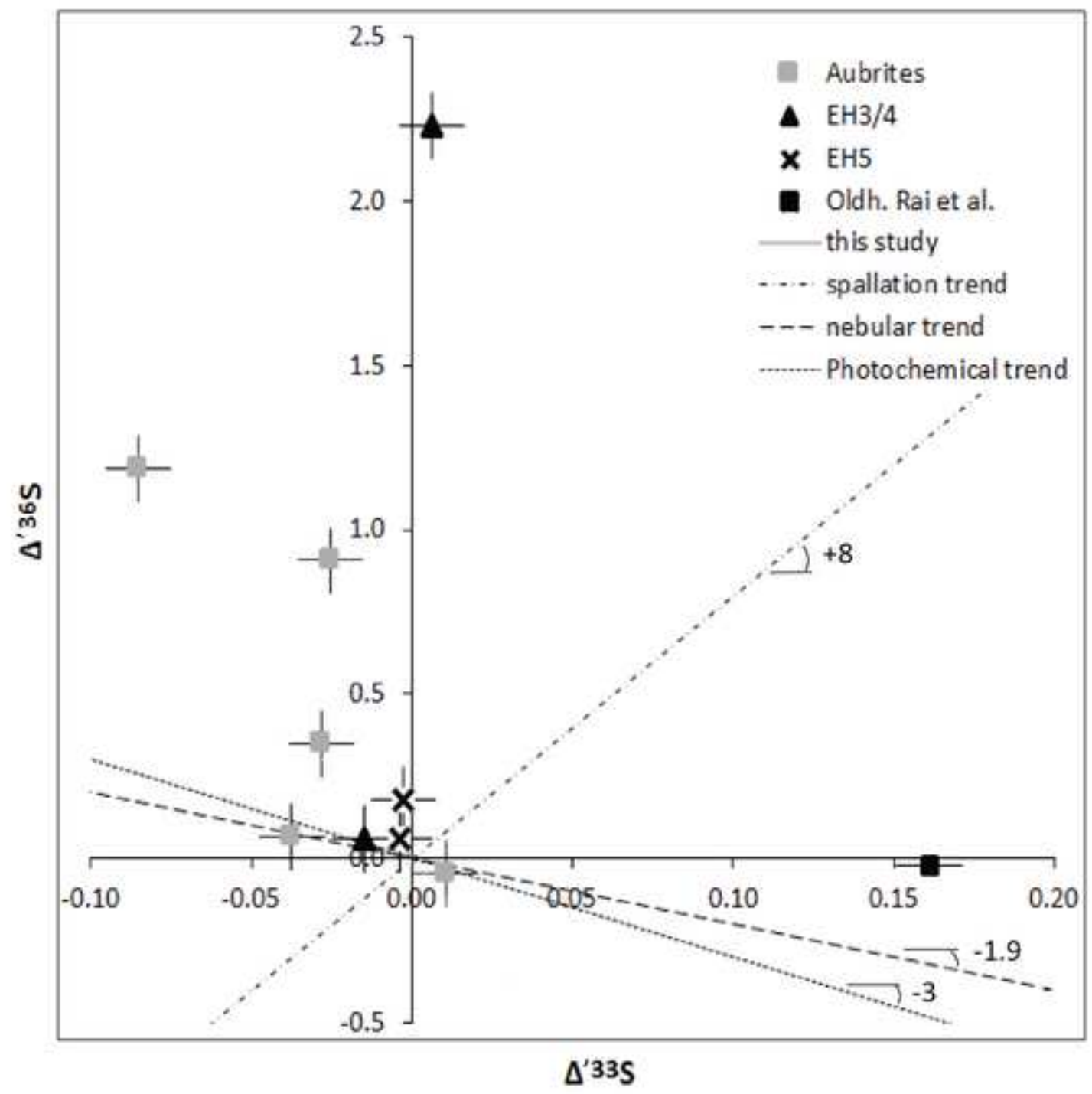


Figure 5

